August 2018

The Geochemistry and Mineralogy of Surface Hydrothermal Alteration at Nesjavellir, SW Iceland

Chase Glenister
University of Wisconsin-Milwaukee

THE GEOCHEMISTRY AND MINERALOGY OF SURFACE HYDROTHERMAL ALTERATION AT NESJAVELLIR, SW ICELAND

by

Chase Thomas Glenister

A Thesis Submitted in

Partial Fulfillment of the

Requirements for the Degree of

Master of Science

in Geosciences

at

The University of Wisconsin – Milwaukee

August 2018

ABSTRACT

THE GEOCHEMISTRY AND MINERALOGY OF SURFACE HYDROTHERMAL ALTERATION AT NESJAVELLIR, SW ICELAND

by

Chase Thomas Glenister

The University of Wisconsin – Milwaukee, 2018

Under the Supervision of Dr. Lindsay McHenry, 2018

Abundant sulfates have been detected by the Mars Exploration Rover Spirit in the Columbia Hills of Mars, consistent with extensive alteration of basalt by hydrothermal processes. This study uses Iceland's Nesjavellir geothermal system as an analogue for Columbia Hills hydrothermal alteration. This terrestrial site is home to a variety of acidic and near-neutral waters that are actively altering the Mars-like basalt of host volcano Mt. Hengill. Hydrothermal features heated by H_2S gas and phase-segregated steam created oxidizing acid-sulfate conditions at the surface with pH values varying between 3.0 and 2.0 and near-boiling temperatures. Mobilization of cations (FeO, MgO, CaO, Na_2O, and K_2O) at these sites is due to the extensive leaching. The resulting alteration products include amorphous silica, anatase, native sulfur, iron sulfides, Ca-, Fe-, Mg-, and Al-sulfates, kaolinite, and montmorillonite, and likely nanophase Fe-oxides. Fe-sulfates were the most common sulfates due to the Fe-rich substrate, and several likely formed from the oxidation of the iron sulfide phases. Due to the ubiquitous presence of iron sulfides and native sulfur in the hydrothermal sites of the Nesjavellir field, it is inferred that reducing conditions are dominant at depth, and conditions become oxidizing either at or near the surface due to interaction with atmospheric oxygen. Two hydrothermal streams at Nesjavellir exhibited a white, pure sulfur coating and an iron-rich red biofilm, respectively. The sulfur coating is attributed to the oxidation of H_2S under near neutral conditions, while the red biofilm forms under acidic, oxidizing conditions. A nearby travertine spring precipitates travertine deposits that preserve microscopic evidence for microbial activity. The diverse variety of environments present in the Nesjavellir geothermal field have formed distinct deposits that resemble several Martian sites in the Columbia Hills, especially the Paso Robles and Arad localities.

TABLE OF CONTENTS

LIST OF FIGURES

LIST OF TABLES

ACKNOWLEDGEMENTS

I would like to start off by thanking my advisors Drs. Lindsay McHenry and Barry Cameron, whose counsel and direction was invaluable in the execution of this project, and for the numerous opportunities with which I was allowed to assist, furthering my geologic expertise in both field and laboratory. Almost all of the research presented here in what feels like a tome could not have been attempted without the near-unlimited use of Dr. McHenry's lab. I would like to thank Drs. Brian Hynek and Tom McCollom and graduate student Sarah Black from University of Colorado – Boulder for their assistance in the field, and Dr. Heather Owen of the UWM Biology Department for the instruction on the use of the SEM. Gratitude goes to Tim Grundl and the School of Freshwater Sciences for the use of their equipment and labs, as well as Dr. Grundl's insight. Fellow graduate students Andy Wanta, Maddy Salo, Sheryl Stephenson, and Megan Barlow were of great assistance in providing context to much of my data. Undergraduate assistants Mark Eskritt, Lisa Mowery, and Jordan Ludyan were invaluable in undertaking the immense amount of lab work. Many thanks to my funding sources: the National Aeronautics and Space Administration (NASA: Habitable Worlds grant NNX15AP15G to McHenry) and UWM Department of Geosciences for the financial support provided.

Finally, many thanks go to the friends, family, and significant other that have supported me through to the end, and a very special thanks to the presenters and producers of the Grand Tour for the support provided.

1. Introduction

Hydrothermal systems are common throughout Iceland and produce a variety of surface hydrothermal features and environments, ranging from acidic fumaroles to neutral hot springs. These various hydrothermal environments can form from a variety of processes that stem from the ascent of geothermal fluid that has been heated by a magma reservoir. This water, upon ascending, undergoes depressurization boiling, which produces steam and other volatiles that can produce fumaroles; conversely, if the steam meets local groundwater, it could heat the cooler water and form steam-heated water. The boiled water, upon reaching the surface, can form hot springs (Stefánsson et al., 2016). The surface expressions of these processes can be dynamic environments, altering and leaching the host rock and producing new minerals. Due to the unique chemistry of these waters, hydrothermal environments host thriving microbial communities that take advantage of the hydrothermal waters (Konhauser and Ferris, 1996; Geptner et al., 2005). Examples of acid-sulfate alteration are abundant in Icelandic hydrothermal systems and are likely analogous to several paleoenvironments on Mars.

The Columbia Hills of Gusev crater on Mars are thought to have been formed by the impacts that formed Gusev crater itself. They were explored by the Mars Exploration Rover (MER) Spirit, which studied various soils and outcrops that appear to represent a variety of hydrothermal environments (Morris et al., 2008; Squyres et al., 2008; Ruff et al., 2011) . These features are limited to specific geomorphic areas, such as topographic lows, the base of slopes, and on slopes, consistent with local, small-scale hydrothermal alteration as opposed to larger, regional-scale processes (McCoy et al., 2008; Wang et al., 2008). The Paso Robles soil class, exposed below the surface dust by the Spirit Rover's broken wheel, has abundant sulfate minerals and amorphous silica, which are thought to indicate an acid-sulfate environment.

Several instances of this soil class occur around the Home Plate area, but in different geomorphic areas of varying size. The differing sizes of these areas may indicate a difference in the abundance of water (Hausrath et al., 2013). Silica nodules located in and near these soils have recently been compared to near-neutral sinter-deposited silica nodules in Chile that are biogenic in nature (Ruff and Farmer, 2016). Examination of similar terrestrial deposits would help further our understanding of the processes that may have once operated in the Columbia Hills. The presence of high-Fe basalt and hydrothermal environments in Iceland allows for comparisons to Martian deposits.

The Nesjavellir geothermal field on the north side of the Hengill volcanic complex in Iceland could provide insight into how the proposed acid-sulfate and near-neutral hydrothermal regimes at the Columbia Hills could have coexisted and interacted. The Hengill edifice is composed of high-Fe basalt, similar to Martian basalts from Gusev crater (McSween et al., 2008; McSween, 2015). The Nesjavellir geothermal field hosts a variety of hydrothermal environments, ranging from acid-sulfate fumaroles and acidic mud pots to near-neutral hot springs and travertine-depositing neutral hot springs. The geothermal field also has several hydrothermal streams, including two with different water chemistry (one acidic, one near neutral) near each other that eventually merge downstream. The mineral assemblages associated with these waters also differ.

To the southeast of the Hengill edifice, the remnants of the volcano Grensdalur (within the Hengill volcanic complex) are being actively altered by the Hveragerdi geothermal field. The Hveragerdi geothermal field has a variety of hydrothermal environments, ranging from acidic to slightly alkaline, and forms silica sinter in the more neutral springs (Geptner et al., 2005; Kaasalainen and Stefánsson, 2012). The interaction between the hydrothermal fluids and the

substrate at these sites and the formation of associated alteration minerals is important to help understand the processes involved in the altering basalt both in Iceland and on Mars.

The primary objectives of this project are to i) assess the mineral assemblages produced from interactions between hydrothermal processes and high-Fe basalt, ii) assess the extent of leaching, and which elements are preferentially leached from the basalt and which are retained in the alteration products, iii) assess the influence of hydrothermal springs and streams on major element mobility and mineral precipitation, iv) understand the controls that the parent lithology and hydrothermal environment have on the secondary mineral assemblages, and v) compare these terrestrial results to deposits in the Columbia Hills of Gusev crater to further our understanding of the processes that were once dominant on Mars.

2. Geologic Background

2.1 Volcanic hydrothermal alteration

The formation of products and deposits by hydrothermal alteration depends on a set of variables including temperature, pressure, rock type, permeability of the rock, fluid composition, and the duration of activity. In the surface expressions of hydrothermal systems, the rock type, fluid composition, duration, and temperature have considerable influence over the minerals formed through alteration (Browne, 1978). These varying conditions can lead to a variety of different products and deposits.

Basaltic substrates exposed to varying hydrothermal conditions yield a range of products. Hydrothermal deposits at Haleakala volcano, Maui, Hawaii contain Fe oxides/oxyhydroxides, jarosite ($KFe^{3+}_3(OH)_6(SO_4)_2$), alunite ($KAl_3(SO_4)_2(OH)_6$), phyllosilicates, and various glass and silica phases (Bishop et al., 2007). The alteration processes observed at these sites are largely

pedogenic and palagonitic at the crater rim and solfataric near the cinder cones in Haleakala, which resulted in different distributions and occurrences of these minerals (Bishop et al., 2007). Looking more towards solfataric processes, the basalts of the Cerro Negro volcano in Nicaragua are being altered by the volcano's sulfur-rich fumaroles into jarosite, natrojarosite, and Mg- and Ca-sulfates (Hynek et al., 2011). The pH values of Cerro Negro's hydrothermal sites vary from 5 to -1. Ultra-acidic conditions form native sulfur, amorphous silica and minor gypsum, while less acidic sites form other sulfate phases (Hynek et al., 2013). This chemical weathering is controlled by the amount of sulfuric acid produced by the fumaroles. Olivine and plagioclase from the substrate are among the first to weather, which allows the freed cations to react with the steam condensates and form a combination of Fe-, Mg-, and Ca-sulfates. This process would eventually completely convert the basalt into amorphous silica, Fe-oxides/hydroxides, and various sulfates (Hynek et al., 2011).

As with Cerro Negro, Icelandic hydrothermal systems also alter basalt that had formed from extensive volcanism. The hydrothermal environments of the Krýsuvík geothermal field on the Reykjanes peninsula exhibit differing pH ranging from mildly alkaline to highly acidic. Low pH environments correspond with areas of high activity, where acid-sulfate mud pots and fumaroles have heavily altered the surrounding area. Minerals found in areas of high activity include kaolinite, covellite, and pyrite (Markússon and Stefánsson, 2011). Areas of medium and low activity towards the exterior of the hydrothermal features exhibit increasing pH. The minerals in these areas reflect the decreasing influence of the fumarole, forming gypsum, anhydrite, and a variety of Cu-sulfates in the area with moderate activity and smectite clay and Fe-oxides and hydroxides in the low activity areas on the margins (Markússon and Stefánsson, 2011). The distribution of the minerals at the Krýsuvík geothermal system show that the supply

of the acidic steam and the extent of the activity were significant controls on the products formed.

The type of rock that hosts a hydrothermal system has a significant influence over the alteration products formed. The basaltic systems discussed previously, among others, form abundant Fe-, Mg-, and Ca-based sulfates when hydrothermally altered. In more felsic settings, such as Bumpass Hell and Sulphur Works of the Lassen hydrothermal system in northern California, Al-sulfates are ubiquitous, interspersed with various Fe-, Mg-, Ca-, and mixed-cation sulfates (McHenry et al., 2017). The abundance of Al-sulfates, especially alunogen, relative to basaltic systems is due in part to the dacitic-andesitic composition of the substrate. The Al-rich substrate, when altered, would allow more Al-sulfates to form than the relatively Al-poor basalts.

Many hydrothermal systems, including the sites previously discussed, have been used as analogues for potential hydrothermal deposits found on Mars. The high-Fe basalt present in Haleakala and Iceland are similar to the protolith basalt on Mars, making these sites excellent for comparison to Martian deposits (Bishop et al., 2007; Cousins et al., 2013; Hynek et al., 2013). Other sites lacking high-Fe basalt, such as Cerro Negro and Mt. Lassen, could still undergo similar processes which would allow comparison to Martian deposits (Black and Hynek, 2017; McHenry et al., 2017).

Terrestrial analogues, however, have several unavoidable limitations, such as an abundance of water and oxygen, which have significant influence over the alteration products. Experimental analogues can help address these limitations, and can produce results closer to Martian deposits than terrestrial analogues alone. Hausrath et al. (2013) and McCollom et al. (2013) altered mineral powders and basalt chips under various hydrothermal conditions under

terrestrial atmospheric conditions in the lab to help constrain and understand the processes forming the various sulfate-rich deposits on Mars. The experiments conducted by Hausrath et al. (2013) yielded results supporting acidic conditions that had enough hydrothermal fluid to allow transport of mobile cations. The experiments done by McCollom et al. (2013) show that when subjected to an acidic fluid, the phenocrysts of a rock quickly dissolve relative to the basaltic glass, which remains relatively intact. The major products of this experiment included amorphous silica, anhydrite, and Fe-rich natroalunite.

2.2 Martian Geology

2.2.1 General Martian Geology

Mars' geologic history is divided into three Periods: the Noachian (4.4-3.8 bya), Hesperian (3.8- 2.0 bya), and Amazonian (2.0 bya to present). Each Period can also be characterized by a global distribution of a dominant surface alteration product, leading to an

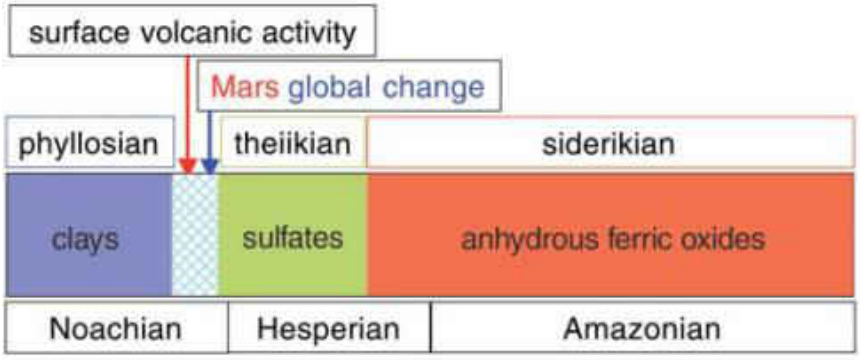

Figure 1- Geologic timescale of Mars, based off surface alteration products. From Bibring et al., (2006).

alternate sequence of eras: the phyllosian (phyllosilicate-rich), the theiikian (sulfate rich), and the siderikian (iron-rich) (Figure 1). The Noachian is defined by widespread non-acidic aqueous alteration in the form of phyllosilicates, suggesting a wet environment (Bibring et al., 2006). Large-scale hydrological features such as valley networks, fan deltas, and paleolake basins are

present in Noachian terranes, indicating that Mars may have had a very active hydrosphere. However, current climate models disagree with a hydrologically dynamic Mars, instead favoring a heavily-glaciated Mars (Davis et al., 2016; Hynek, 2016). The end of the Noachian is marked by widespread volcanism and a drastic change in the Martian surface environment from moderately alkaline to acidic. The escape of atmospheric gases from Mars' gravity, assisted by solar wind erosion and bolide impacts from the Late Heavy Bombardment (LHB), eroded the early Martian atmosphere, changing the climate in the process (Bibring et al., 2006; Barlow, 2010).

As the LHB declined, Martian volcanism intensified, introducing more sulfur dioxide into the atmosphere as a by-product of volcanic outgassing (Barlow, 2010). The introduction of sulfur dioxide and the general desiccation of the surface allowed for the formation of the widespread sulfate alteration deposits characteristic of the Hesperian Period (Bibring et al., 2006). The abundant water of the Noachian became more restricted and increasingly acidic due to interactions with sulfur dioxide (Barlow, 2010). Eventually, the remaining water evaporated and the thinner atmosphere diminished to present-day levels (Barlow, 2010; Bibring et al., 2006). These conditions promoted alteration driven by non-aqueous atmospheric processes, forming the Amazonian Period's characteristically red ferric oxide deposits (Bibring et al., 2006).

The Martian surface was heavily influenced by volcanism during the Noachian, which became even more widespread during the Hesperian. Martian mafic igneous rocks differ depending on the age of the terrane, with alkaline rocks common in ancient terranes and tholeiitic rocks in younger terranes, suggesting global magmatic evolution (McSween, 2015). Mountains located in the southern polar region of Mars were most likely subglacial volcanoes (Ghatan and Head, 2002). These subglacial environments would have been promising locations

for hydrothermal activity, since terrestrial counterparts undergo alteration from aqueous interaction with melt water (Cousins et al., 2013).

Bolide impacts also formed hydrothermal systems on Mars. The impactor would create an impact melt sheet, which would heat the local groundwater to form hydrothermal systems (Abramov and Kring, 2005). Toro crater of Syrtis Major is an example of this process, and has hydrothermal deposits associated with its central uplift (Marzo et al., 2010). The Columbia Hills of Gusev crater underwent the same process, initially forming from a central uplift and subsequently inundated with impactor ejecta and volcanoclastic material, which was then altered (McCoy et al., 2008; Filiberto and Schwenzer, 2013). Interestingly, Meridiani Planum (studied by MER Opportunity) has similar mineral assemblages, but a very different proposed formation pathway. The deposits present there have been attributed to episodic sedimentary processes, evaporation, and subsequent desiccation (Squyres et al., 2004).

The search for extraterrestrial life has made extensive headway in possible once-habitable environments on Mars. Noachian-aged phyllosilicate deposits are promising sites for exploration, as the abundant and thick deposits are indicative of the widespread presence of abundant water (Bibring et al., 2006; Bishop et al., 2008). Phyllosilicate deposits in Mawrth Vallis exhibit a change in iron from Fe^{3+}/Mg-rich phyllosilicates to Fe^{2+}-rich phyllosilicates, which are capped by Al/Si-rich phyllosilicates, which in terrestrial deposits would be consistent with multiple aqueous phases depositing and then altering the deposits, likely related to biological activity (Bishop et al., 2013). Furthermore, pre-biotic chemistry or primitive life could have taken advantage of the reaction surfaces provided by the soft clay. Traces of biological activity could have been preserved by the fine-grained clay and the cooler, drier environment of Mars (Bishop et al., 2013).

As the water content of Mars slowly diminished, and volcanism increased, the resulting acidic waters could have still been a habitable environment. Acidic hydrothermal environments on Earth can be hosts to thriving microbial communities, whether in black smoker communities or in surface hydrothermal features (Inskeep et al., 2004; Geptner et al., 2005; Westall et al., 2013). The Martian surface has a global prevalence of S and Fe, which suggests that potential microbial communities would have likely exploited the abundant Fe and S using Fe- and S-based metabolic strategies and/or methanogenesis (Nixon et al., 2013). Hydrothermal features in Gusev crater include likely silica sinter precipitates that appear to have formed through biological processes based on comparisons to the El Tatio geothermal field (Ruff and Farmer, 2016). As the availability of water on the Martian surface continued to diminish, microbial life could have continue to thrive in the subsurface, where aquifers would outlast the evaporating surface water (Westall et al., 2013). These subsurface environments could still exist today, but the potential conditions and energy sources would be difficult to analyze without drilling into the subsurface (Nixon et al., 2013).

While the possible environments and conditions necessary for life may vary, a constant is the presence of liquid water. At the time the MERs were deployed, finding evidence for liquid water was the first step to identifying potentially habitable environments, hence the MER program's strategy to "follow the water" (Arvidson et al., 2008; Grotzinger, 2009). While this "water-first" strategy is still at the forefront of the search for life, it has expanded to include several other indicators of life, such as the presence of atmospheric O_2 as an indicator of photosynthesis, evidence of complex organic-based molecules as indicators of potential biological processes, and the presence of methane as a biological marker. The Curiosity rover, while currently "following the water", is also searching for several of these indicators

(Grotzinger, 2009). The future Mars 2020 rover will take this a step further, looking for evidence of actual biological activity, such as possible fossils and byproducts of biological activity, and storing samples with these indicators for future collection and analysis. Much of this work will be compared to Earth-based processes and deposits. This helps us understand the Martian environment and its processes within the context of an environment we understand, and helps put the existence of life on our planet into perspective (Des Marais et al., 2008). The exploration of Mars, and other planets, both in the solar system and beyond, is driven by the desire to understand our place in the universe, to determine if life is an oddity or common, and to evaluate the possibility that we are not alone in this universe. The exploration and analysis of these various environments follow the 2015 NASA Astrobiology Strategy roadmap (Achenbach et al., 2015).

2.2.2 Columbia Hills, Gusev Crater

The Columbia Hills of Gusev crater, investigated by MER Spirit, likely formed during the Late Noachian (McCoy et al., 2008). The Columbia Hills is dominated by basaltic material, some of which has been heavily altered through both isochemical and acid-sulfate alteration (Golden et al., 2005; Morris et al., 2008). Isochemical alteration is indicated by abundant hematite, goethite, and nanophase ferric iron oxides, and involves little change in bulk composition, whereas the abundant sulfates present at multiple sites suggests non-isochemical acid-sulfate alteration (Golden et al., 2005). These zones of alteration are typically found in specific geomorphic settings, which include local topographic lows, the base of steep slopes, near large outcrops, and on slopes (Figure 2). The differences in geomorphic environments could help explain differences in the hydrothermal environment, and also demonstrate that these

deposits most likely formed from local, small-scale hydrothermal processes rather than from larger-scale regional processes (Wang et al., 2008).

One of Spirit's study sites, Home Plate, is a small (~90 m across) plateau composed of layers of volcaniclastic rocks that can be divided into two main units; a coarse-grained lower unit

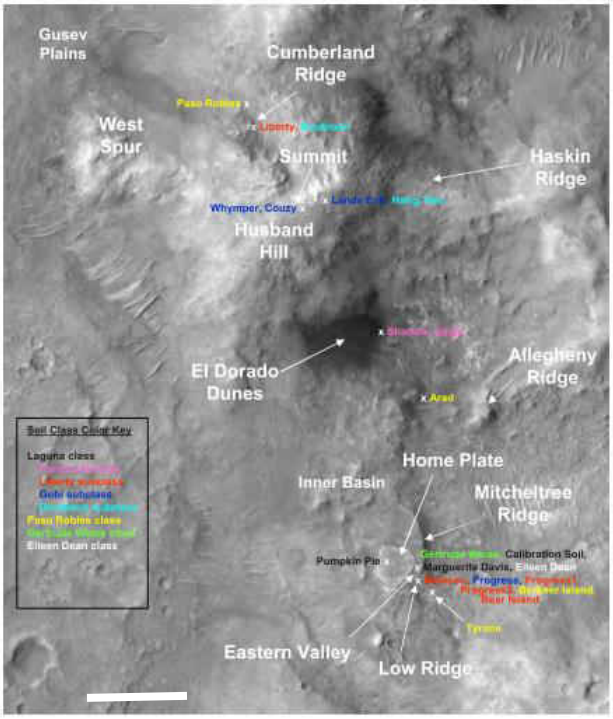

Figure 2- HI-RISE image of the Columbia Hills, with the locations of various soils and rock classes. From Ming et al. (2008). White bar is 100 km. Yellow labels are sites containing Paso Robles class deposits.

and a fine-grained, laminated upper unit, both of alkali-basaltic composition. A bomb sag feature in the lower unit suggests that the unit was wet during emplacement, leading to the interpretation that these deposits were likely caused by a phreatomagmatic event (Squyres et al., 2007; Manga et al., 2012). The eruption could have been initiated by the introduction of magma to a shallow, briny groundwater aquifer rich in Cl, Br, Na, and other cations (Schmidt et al., 2008). After deposition of the volcanic material of the lower coarse-grained unit, aeolian processes reworked the finer material into the fine-grained upper unit (Squyres et al., 2007).

When these sites were visited by Spirit, soils and rocks were assigned to classes based on characteristic mineralogy and probable formation mechanism. The Paso Robles soil class is defined as being sulfur- and ferric sulfate-rich, and is present in the Paso Robles, Arad, and Tyrone localities (Figure 2). The mineral assemblages present in Paso Robles and Arad are heterogeneous across the area, but are fairly homogenous in Tyrone. This trend is attributed to Paso Robles and Arad possibly being formed from acid-sulfate fumaroles, while Tyrone likely formed under higher water:rock ratio conditions (Hausrath et al., 2013; Wang et al., 2008). The assemblages present in these soils include a variety of Mg and Ca sulfates, hematite, amorphous silica, and ferric sulfates, which include ferricopiapite ($Fe_5(SO_4)_6O(OH) \cdot 20H_2O$), jarosite, rhomboclase ($(H_5O_2)Fe^{3+}(SO_4)_2 \cdot 2H_2O$), and anhydrite, among others. The environment at Tyrone could have been habitable for microbial life (Wang et al., 2008).

After the formation of Home Plate, the area was likely subjected to a dynamic, laterally variable hydrothermal system. The eastern side of Home Plate (Eastern Valley and Tyrone) was subject to a higher temperature regime than the western side (Barnhill and PecanPie) (Figure 2). As a result, the two sides have different distributions of iron-based mineral phases. The higher temperatures formed Fe^{3+} sulfate soils and hematite-rich outcrops due to acid-sulfate fumarolic/hydrothermal activity (Morris et al., 2008; Schmidt et al., 2009).

Just beyond Home Plate, Spirit analyzed outcrops and soils that were light-toned and silica-rich in and near the Eastern Valley and Tyrone localities (Figure 3). After detailed analyses of the soils and outcrop nodules, it was established that the high silica concentration was due to opaline silica, and that the soils were depleted in almost all other major elements. The opaline silica was often found with ferric sulfates, a likely hydrothermal product. Based on these observations, these deposits were established as hydrothermal (Squyres et al., 2008). Several hypotheses were proposed to explain the formation of these siliceous nodules and soils. Morris et al. (2008) suggested that they were the result of leaching under acid-sulfate conditions, implying high water-to-rock ratios. Squyres et al. (2008) corroborate this, but suggest fumarolic activity as a possible mechanism for leaching. However, Ruff et al. (2011) argue that the features of these nodules are not characteristic of leaching, but more similar to sinter deposits of near-neutral geysers and hot springs.

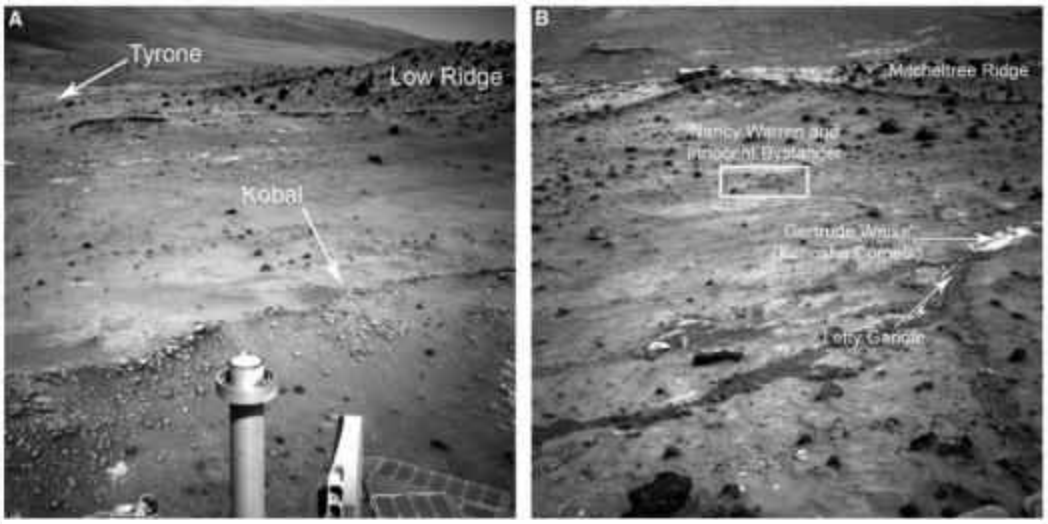

Figure 3- Navcam images of the area surrounding and in the Eastern Valley locality. A) View to the southeast, looking at the sampled nodules (Kobal) and viewing the Tyrone locality. B) View west, looking at the trench excavated by the rover. Image taken from Squyres et al. (2008).

The variation present in the hydrothermal mineral assemblages of the Home Plate region suggests a variety of hydrothermal environments affecting Home Plate. While the temporal

relationship between these sites is not known, the deposits' spatial relationship implies a wide-ranging dynamic hydrothermal system, possibly related to the hydrovolcanism that formed Home Plate (Rice et al., 2010).

2.3 Icelandic Geology

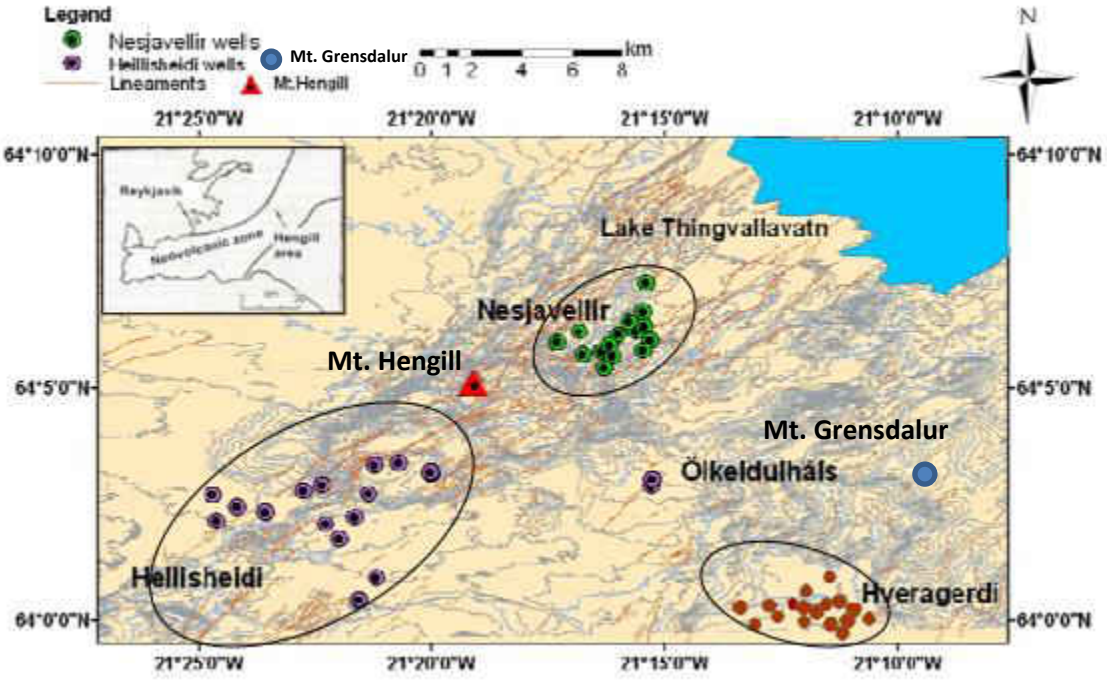

Figure 4- Locations of the volcanic edifices Hengill and Grensdalur and the Nesjavellir, Hveragerdi, and Hellisheidi geothermal fields. Adapted from Mutonga et al (2010).

Iceland is located where a mantle plume impinges on the Atlantic mid-ocean ridge, resulting in a volcanically dynamic island. Iceland is separated into Northern, Western, and Eastern Volcanic Zones, all of which are a part of the Neovolcanic Zone, the subaerial extension of the Mid-Atlantic Ridge (Foulger and Toomey, 1989). The mantle plume, in conjunction with the Mid-Atlantic rifting, has produced subaerial volcanism for at least 16 Myrs. Mechanical effects due to glacial loading and unloading could also affect the magma production of the mantle (Maclennan et al., 2002). The glaciations, along with the rifting associated with tectonic

processes, has considerable influence over the placement and formation environment of the Icelandic edifices (Bourgeois et al. 1998).

2.3.1 Hengill Volcanic Province

The Hengill volcanic complex (HVC) is located at the meeting of three different tectonic zones, creating a triple junction that produces favorable conditions for upwelling magma (Jousset et al., 2011) (Figure 4). This junction is created by the spreading at the Reykjanes Peninsula, the Western Volcanic Zone, 25 km east of Reykjavik, and the South Island Seismic Zone, which is a transform fault expressing the transition from the Western Volcanic Zone to the Eastern Volcanic Zone (Jousset et al., 2011; Verney-Carron et al., 2015). The HVC is thought to have originally formed ~500 kyrs ago from magma migration from nearby Grensdalur, which is currently the heat source for the nearby Hveragerdi geothermal field (Trønnes, 1990).

Subsequently, Hengill accumulated pillow basalt and hyaloclastite layers due to glacial interactions and produced 25-30 cubic kilometers of hyaloclastites and lava, with the majority of material being hyaloclastites. Maximum productivity occurred during the isostatic rebounds of the deglaciation periods 130 and 10 kyrs ago (Trønnes, 1990). The volcanic material produced ranges in composition from picritic basalt to rhyolite, with the mafic material being overwhelmingly dominant.. Olivine tholeiite was the first to erupt, followed by picrite basalts and then plagioclase-phyric pillows (Hardardottir, 1983). Since its formation, the Hengill edifice has been affected by the Nesjavellir geothermal system. This study focuses on the alteration of the more recent tholeiitic lava flows that form the lower slopes of the edifice (Figure 4).

2.3.2 The Nesjavellir geothermal field

Figure 5- Hydrothermal fumaroles and springs of the Nesjavellir geothermal field flowing towards Lake Thingvallavatn to the north.

The Nesjavellir geothermal field is located on the northern side of Hengill and uses fissure swarms from previous eruptions as outflow zones (Franzson et al., 2005) (Figure 5). Nesjavellir originally formed from high-temperature activity less than a hundred thousand years ago, and its main water source is the nearest glacier, Langjökull, rather than local meteoric water (Arnason et al., 1969; Mutonga et al., 2010). The water is heated by a magma reservoir 2-4 km beneath the Hengill Volcanic Complex, where it is boiled and ascends to the surface (Foulger and Toomey, 1989; Mutonga et al., 2010). During boiling, the resulting water vapor takes in CO_2 and other volatiles and alters the rocks above as it percolates to the surface.

Due to differences in rock temperature, the waters form different alteration zones, with distinct mineral assemblages (Franzson, 2000; Mutonga et al., 2010). At depth, these zones vary from zeolite and smectite clay to chlorite, epidote, and actinolite/amphibole (Mutonga et al., 2010). On the surface, hydrothermal waters alter surface basalts to form a variety of products,

from clays and various silica phases to various sulfates and hematite deposits (Browne, 1978). The Nesjavellir geothermal field, located on the margins of the Hengill Volcanic Complex, is subject to the ebb and flow of heat from the magma reservoir for the Hengill edifice. The geothermal field was cooling before the present high-temperature thermal regime started less than 100 kyrs ago (Franzson, 2000).

2.3.3 Grensdalur volcanic province

Grensdalur is located to the southeast of the HVC and was the original focus of volcanism and accretion related to the Hengill triple junction. Initially forming ~700 kyrs ago, the Grensdalur edifice was heavily influenced by glacial activity, forming a volcanic stratigraphy reflecting the subglacial environment into which it erupted. The base of the edifice is composed of hyaloclastites interspersed with brecciated pillow fragments, followed by alternating layers of basaltic lava flows and hyaloclastite layers, reflecting changes in the glacial environment. The majority of the volcanic material varies from olivine tholeiite to tholeiite, with a single rhyolitic dike. Grensdalur eventually migrated eastward due to the tectonic rifting of the WVZ, and the magma fueling Grensdalur eventually migrated to the northwest to what would be the Hengill edifice (Wangombe, 1987). The volcano has since ceased activity and has eroded from glacial erosion and hydrological processes. The erosion is deep enough to reveal the intrusions and dikes that had once transported magma (Foulger and Toomey, 1989). The remains of Grensdalur are currently host to the Hveragerdi geothermal system.

2.3.4 The Hveragerdi geothermal field

The Hveragerdi geothermal field is located on the slopes of the remains of Grensdalur, and is currently heated by a combination of Grensdalur's remnant magma and adjacent Hengill's

magma reservoir (Arnason et al., 1969; Mutonga et al., 2010). The hydrothermal waters currently altering the extinct volcano are sourced at Langjokull, the same glacial source as the Nesjavellir geothermal field. The water is thought to have initially been heated at depth at Hengill, with many volatiles being boiled off, then traveling southeast in the subsurface to where it emerges at Grensdalur (Arnason et al., 1969). The geothermal system contributes to erosion, and has exposed a chlorite-bearing fossil hydrothermal system over a 3 km area on the slopes of Grensdalur (Wangombe, 1987; Mutonga et al., 2010). At depth, the current geothermal system is predominately alkaline to sub-alkaline, with a few sites approaching neutral (Kaasalainen and Stefánsson, 2012), though acid-sulfate fumaroles and mudpots still occur locally at the surface. Silica sinter deposition has occurred at several springs, and has been used to study hydrothermal fossilization of microbial material through silicification (Geptner et al., 2005).

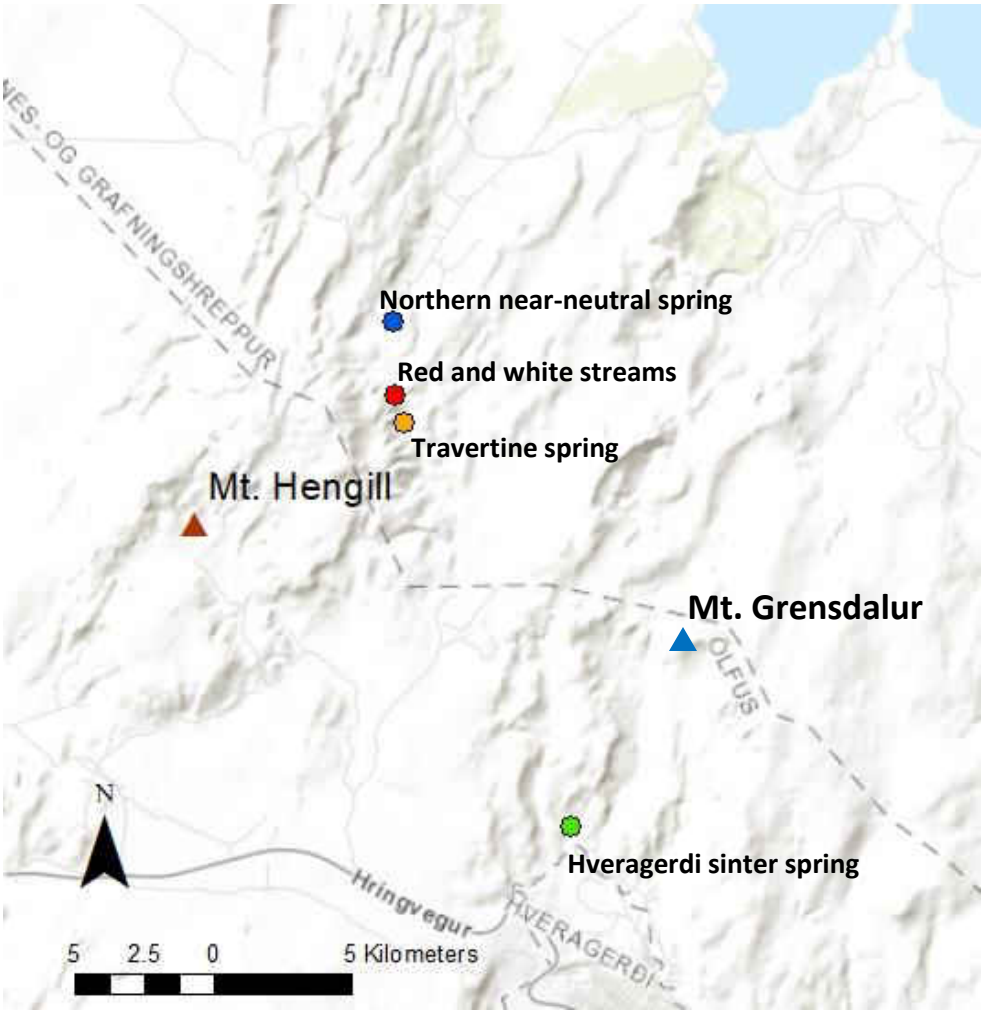

Figure 6- Sample sites in southwest Iceland.

3. Methods

3.1 Field Work

In August 2016 and June 2017, we collected samples from a variety of hydrothermal features in the Nesjavellir and Hveragerdi geothermal fields (Figure 6). This study focuses on several sites south of the Nesjavellir power plant (Figure 7). The first is a hydrothermal area with hot springs and fumaroles, where a near-neutral stream with white precipitates (the "white stream") and an acidic "red stream" meet (Figure 8). Southeast of this site is a travertine-

depositing hot spring (Figure 9). Another hydrothermal area north of the white and red hydrothermal streams is a near-neutral hot spring altering the surrounding basalt (Figure 10). Altered soils and precipitates were collected from these features, and more pristine samples of the basalt substrate were hammered off nearby outcrops away from geothermal features to compare the altered material to the less altered substrate. Collected samples are described in terms of color, temperature, GPS coordinates, and pH where nearby water was available for testing. Samples were stored and transported back to the lab in small plastic bags.

	Site	Sample	Type	Description	Temperature (°C)	pH
2013	Hveragerdi sinter spring	IH1311	Precipitate	Layered deposits near the hot spring		
		IH1312	Water	Hydrothermal water from the hot spring	90.0	8.0
		IH1313	Soil	Orange layered rocks from pool wall		
		IH1314	Precipitate	White, fibrous coating precipitate out of cold stream	10.3	5.5
2016	Northern near-neutral hot spring	IN1601	HL + WS	Boiling hot spring	82.2	5-5.5
		IN1603	Altered soil	White heavily leached rock nearby	21.7	
		IN1604	Altered soil	Orange soft surface coating on adjacent rock	22.9	
		IN1605	Precipitate	Orange surface precipitate with crinkly edges near fumarole on S side of hot spring	42.8	
		IN1606	Precipitate	White sulfate surface precipitate- cauliflower-like	46.8	
		IN1607	Altered soil	Dark grey dirt a few cm below IN1605 and IN1606	90.3	2.5
	Acidic and near-neutral springs and streams	IN1608	HL + WS	Cool stream with white soft precipitate	22.9	5-5.5
		IN1609	Precipitate	White sludge coating rocks in stream of IN1607	22.9	
		IN1610	HL + WS	Red stream (hotter water)	63.5	3.5
		IN1611	Precipitate	Red crust on rocks in red stream	66.5	
		IN1612	Altered soil	Directly next to red waterfall		
		IN1613	HL + WS	Bubbling, clear hot spring upstream from red stream	93.2	2.0
		IN1614	Precipitate	Honey-comb grey coating over dark grey mud	68.5	
		IN1615	HL	Confluence of white and red streams	21.3	6.0
2017	Southern neutral hot spring and acidic mud pot	IN1701	HL + WS	Large neutral hot spring	67.0	7.0
		IN1702	Precipitate	Travertine levee along outflow stream margin from IN1701 pool.		
		IN1703	Precipitate	Fossil but recent travertine crust further down travertine mound. Dark surface, orange interior		
		IN1704	Precipitate	Fossil travertine- thick with layers, orange		
		IN1705	HL + WS	Acid bubbling mud pot E of travertine mound	82.6	2.5
		IN1706	Mud	Mud from pool of IN1705. Light beige, watery		
		IN1707	Mud	Directly adjacent to IN1705 pool, light orange clayey mud.	92.1	
		IN1708	Mud	2 m from IN1705 pool, red mud next to rock.	44.8	
	Acidic and near-neutral springs and streams	IN1709	HL + WS	Bubbling hot spring in large pool at NW end of "island" between white and red streams	81.7	5.0
		IN1710	Precipitate	Light yellow thick coating on rocks in stream, several cm thick		
		IN1711	HL + WS	Water from stream with IN1710 precipitate	9.3	4.5
		IN1712	HL + WS	Downstream along white stream, above confluence with red stream	14.5	5.0
		IN1713	Precipitate	White and yellow precipitate on wall directly adjacent to IN1712 stream	57.1	
		IN1714	HL + WS	Non-thermal spring at top of drainage above IN1710 and IN1711	4.8	5.0
		IN1715	HL + WS	Confluence of white and red streams	24.2	5.0
		IN1716	HL + WS	Red stream- right upstream of confluence	64.7	4.0
		IN1717	HL + WS	Source of red stream- higher up in the valley	94.9	2.0
		IN1718	Mud	Mud from pool of IN1717. Dark grey, sticky, thick.		
	Hveragerdi sinter	IH1701	HL + WS	Water from 2013/2014 sinter depositing site, boiling under rocks.	99.4	7.7
		IH1702	Precipitate	Yellow and white precipitate over IH1701.	71.4	

Table 1- List of samples collected from the Nesjavellir geothermal field during the 2016 and 2017 field seasons color coded and categorized by site. HL=Hydrolab, WS= Water Sample. Light blue- northern hot spring, yellow- near neutral stream, red- acidic stream, green- confluence water, orange- neutral travertine-depositing hot spring, dark blue- acidic mud pot, gray- hot spring, dark red- acidic mud pot uphill from hydrothermal streams, bright green- neutral sinter depositing hot spring in the Hveragerdi geothermal field.

Hydrothermal waters from targeted features were sampled to ascertain their hydrochemical properties and conditions. Water samples were collected using a bottle duct-taped to a Jacob's Staff, and were tested onsite for temperature and pH with a temperature probe and pH paper. An HL4 Hydrolab sonde was then used to measure the pH, salinity, oxidation/reduction potential, total dissolved solids, and specific conductivity of the geothermal waters (Figure 7). Analyses were conducted in situ for water below 50°C. Above 50°C, water was poured into a small container and allowed to cool prior to analysis. Water samples were each

filtered into two 60 mL sample bottles using a 0.2 micron cellulose filter. One bottle was acidified with 4 N nitric acid for further cation analysis, while the other bottle was left as is for anion analysis. Field bicarbonate titrations were conducted using 0.02 N hydrochloric acid titrant for neutral samples and 0.02 N sodium hydroxide titrant for acidic samples. Samples for which no bicarbonate titration was possible had their bicarbonate concentrations back-calculated from their molar equivalences (meq/L), assuming the water samples are electrically balanced. The pH meter used for titration was a Fisher Scientific Accumet hand-held meter that uses a saturated silver chloride reference solution. Chemetrics Fe^{2+} ampoules were used to estimate the amount of Fe^{2+} present in the water at the time of sampling.

3.2 Mineralogy and geochemistry

Alteration and precipitated products were analyzed and characterized using X-ray Diffraction (XRD) and X-ray Fluorescence (XRF). Samples collected from the travertine deposits were also analyzed using the scanning electron microscope's (SEM) energy-dispersive X-ray spectrometer (EDS) to determine the element abundances and distributions in samples of the travertine wall. For XRD analysis, altered soils and precipitates were first dried in aluminum trays over a few days. Dried samples were then ground using an agate mortar and pestle until the resulting powder was fine enough to fit through a 230-mesh (63-micron) sieve. The sieved portion was discarded and the remaining portion was retained for analysis. During this process water and heat were avoided to prevent further alteration or dissolution of the samples. The fine powders were then loaded into a cavity mount, smoothed, and analyzed using a Bruker D8 Focus XRD (Cu Kα target, 0.6 mm divergence and antiscatter slits, a nickel filter, a 0.1 mm detector slit, a 2theta range of 2° to 60°, a 0.02° 2theta step size with 1 s/step, and a scintillation detector) following the methods of McHenry et al. (2017). Resulting scans were compared against the

International Centre of Diffraction Data's (ICDD) PDF-2 database using the EVA software from Bruker.

The altered products and substrate were analyzed by X-ray Fluorescence (XRF) to determine their major and minor element compositions. Large samples (e.g. substrates) were broken down using a hammer. Samples were powdered using a tungsten carbide shatterbox. The powdered samples were heated overnight at 105°C to evaporate excess water, and then a portion was ashed at 1050°C in a muffle furnace to determine the loss-on-ignition (LOI). 1.000 g of the remaining powder was then mixed with 1 g of ammonium nitrate and 10.000 g of a 49.75c% lithium tetraborate-49.75% lithium metaborate-0.5% lithium bromide flux. The mixture was fused using a Claisse M4 fluxer, and the resulting glass beads were analyzed for major, minor, and some trace elements using a Bruker S4 Pioneer WD-XRF following the methods of McHenry et al. (2017). Concentrations of major and minor elements SiO_2, TiO_2, Al_2O_3, Fe_2O_3, MnO, MgO, CaO, Na_2O, K_2O, P_2O_5 and trace elements Y, Zr, Nb, V, Zn, Ni, Cr, Ce, Sr, and Ba were evaluated using a calibration based on eleven USGS igneous and sedimentary rock standards. An element's concentration is considered detectable if the concentration is double the lower limit of detection and has less than 12% or 2% statistical error for the trace and minor elements and the major elements, respectively (Byers et al., 2016).

The travertine-depositing hydrothermal site was the primary focus for SEM analysis, because of its neutral waters and the morphologically unique deposits. Pieces were broken off larger samples and adhered to SEM mounts using carbon glue, carbon paint, and occasionally copper tape. Mounted samples were sputter coated with an Emitech K575X Sputter coater to attain an iridium coating 12 nm thick and analyzed using the secondary electron detector on the Hitachi S-4800 SEM in the UWM Biological Sciences department. Other portions of the samples

were studied using a Bruker Quantax ESPRIT EDS system. These portions were adhered to an SEM mount using carbon glue and then carbon coated using an Edwards vacuum coating unit.

Water samples were analyzed using an Atomic Adsorption analyzer (AA) and an Ion Chromatography analyzer (IC) according to the methods of Standard Methods for the Examination of Water and Wastewater, 17th ed. (1989) and Ion Chromatography (1982), Ion Chromatography (1989), and Ion Chromatography in Water Analysis (1988). The samples were analyzed at the School of Freshwater sciences at UW-Milwaukee. The AA determines the concentrations of Ca^{2+}, Mg^{2+}, Na^{+}, and K^{+} in the water, while the IC determines the concentrations of SO_4^{2-} and Cl^{-}.

Figure 7- Author and co-advisor using a Hydrolab sonde in the field.

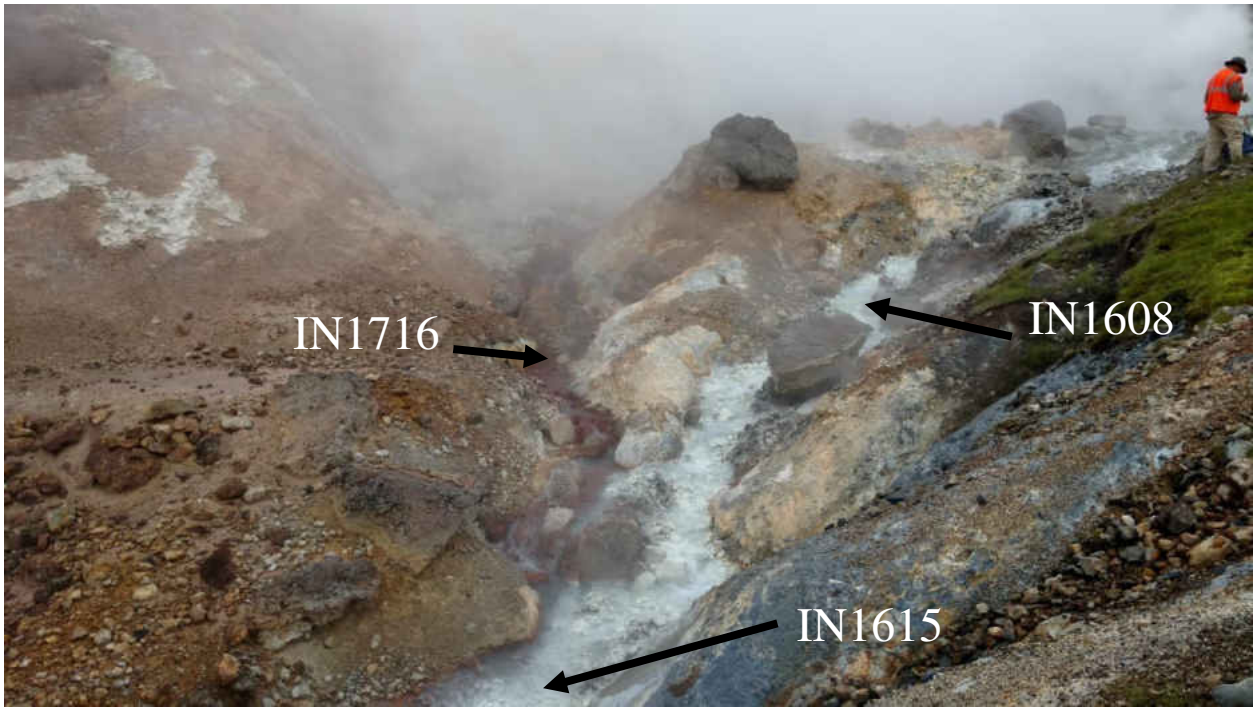

Figure 8- The acidic red stream on the left flowing into the near-neutral white stream on the right.

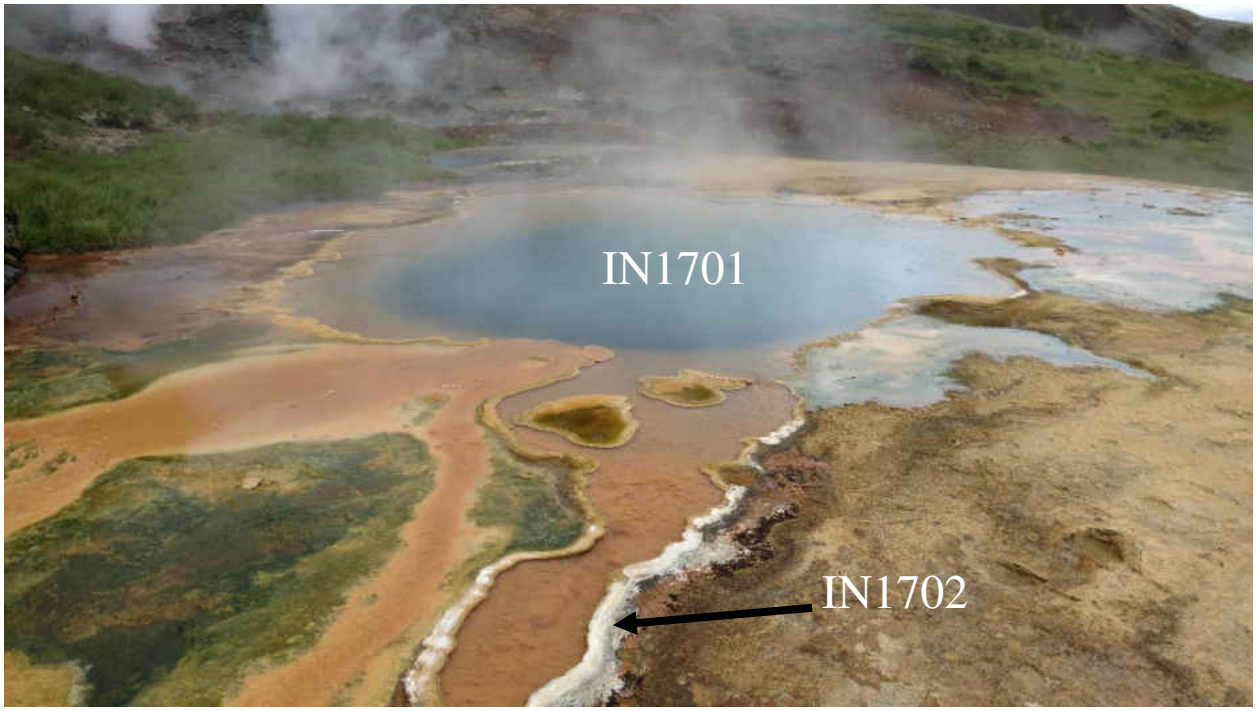

Figure 9- A neutral travertine-depositing hot spring. The travertine forms canals that funnel the water downhill.

Figure 10- Various sample sites on the northern slope of Hengill, with sample IDs indicated. a) A near-neutral (pH 5.6) bubbling hot spring with altered soil and sulfates along the margin. b) Portion of red stream (shown in figure 7b) above the confluence water with the red biofilm and leached soil nearby. c) Acidic bubbling spring flowing into the red stream. d) White stream with white coating and precipitates on bank. e) Acidic mud pot upstream from the confluence of the two streams. f) Two small streams flowing into the white stream, with a white coating.

4. Results

4.1 XRD

Northern near-neutral hot spring

		IN1603	IN1604	IN1605	IN1606	IN1607
		S	S	P	P	S
	Temperature (°C)	21.7	22.9	42.8	46.8	90.3
Misc. phases	Am. Silica	XXX		XX		
	Tridymite	X				
	Anatase	X		X		
	Plagioclase					X
	Montmorillonite		XX	XX		XX
	Kaolinite		+			
Fe-sulfides	Pyrite					XX
Ca-sulfates	Gypsum			XX		
Al-sulfates	Alunogen			X		XX
Fe-sulfates	Halotrichite				XXX	
	Natrojarosite			XX		

Table 2- Minerals forming in and near the northern near-neutral hot spring. S- Soil, P- precipitate. XXX- abundant, XX- common, X- present, +- rare.

The mineral assemblages of the near-neutral (pH 5.6) hot spring are presented in Table 2. The surrounding soil (samples IN1603, IN1604, IN1607) has abundant amorphous silica and clay phases. The high-temperature silica phase tridymite is present in nearby white soil deposits (IN1603). The orange precipitate (IN1605) contains a variety of sulfates, including natrojarosite ($NaFe(SO_4)_2(OH)_6$). The smectite, amorphous silica, and anatase likely reflect the soil under IN1605, incidentally collected with the precipitate. The white precipitate (IN1606) is pure halotrichite ($FeAl_2(SO_4)_4 \bullet 22H_2O$). Dark grey soil (IN1607) occurs at a few cm depth, and like the other soil samples contain clays. The dark grey soil also contains pyrite and alunogen ($Al_2(SO_4)_3 \bullet 17H_2O$). The plagioclase present in the soil is a primary igneous phase from the volcanic substrate, and not an alteration product.

Acidic and near-neutral streams

		White Stream			Red Stream			Mud Pot	Substrate
		IN1609	IN1710	IN1713	IN1611	IN1612	IN1614	IN1718	IN1616
		P	P	P	P	S	P	M	Sub
	Temperature (°C)	15	9.3	57.1	59.3	59.3	68.5	94.9	Amb
Misc. Phases	Am. Silica						XXX		
	Anatase					XX			
	Plagioclase							X	XXX
	Clinopyroxene								XXX
	Montmorilonite	+	X						
	Kaolinite					XXX		X	
	Sulfur	XXX	XXX				XX	XX	
Sulfides	Pyrite					X	X	XX	
	Marcasite						X		
Al-sulfates	Alunogen						XX	X	
	Aluminite						XX		
Ca-sulfates	Barite							XX	
Mg-sulfates	Pickeringite			XX					
	Magnesiocopiapite			XX					
Fe-sulfates	Rhomboclase						XX		
	Melanterite						X		

Table 3- Minerals forming in and near the acidic red stream and the near-neutral white stream. Yellow indicates samples collected in and near the white stream, red were collected in and near the red stream, dark red is an acidic mud pot up the valley, and gray is the substrate. S- soil, P- precipitate, M- mud, Sub- substrate, Amb- ambient temperature. XXX- abundant, XX- common, X- present, +- rare.

The mineral assemblages present in and near these streams are presented in Table 3, and several representative XRD patterns are presented in Figure 11. The white coating characteristic of the white stream (pH 5.82) (IN1609 and IN1710) is composed almost entirely of native sulfur. The white precipitate (IN1713) in a steam-heated area on the banks of the white stream just above the confluence is composed of the Mg-sulfates pickeringite ($MgAl_2(SO_4)_4 \cdot 22(H_2O)$) and magnesiocopiapite ($MgFe_4(SO_4)_6(OH)2 \cdot 20(H_2O)$). Pickeringite (Mg-bearing) and halotrichite (Fe-bearing) are difficult to distinguish using XRD, as are magnesiocopiapite and ferrocopiapite, thus the exact mineral assemblage is uncertain. The red biofilm characteristic of the acidic stream (pH 3.19) is X-ray amorphous. Due to the red coloring of the coating, the high concentrations of iron measured by XRF, and the high backgrounds in the XRD pattern (likely

due to iron fluorescence), nanophase iron oxides/hydroxides are likely present. The biofilm textures of this coating (IN1611) are consistent with a microbial origin. A portion of the embankment (IN1612) being cut into by the red stream contains residual minerals anatase and kaolinite, with minor pyrite. The acidic hot spring flowing into the red stream has abundant sulfates precipitating on its margins, including the Fe-sulfate phases rhomboclase and melanterite ($FeSO_4 \cdot 7(H_2O)$) (IN1614). Pyrite, marcasite, native sulfur and amorphous silica are also observed in these precipitate samples. The substrate basalt (IN1616) used for XRF analysis is composed mostly of plagioclase and clinopyroxene.

Travertine-depositing hot spring and associated acidic mud pot

		Travertine spring			Acidic mud pot		
		IN1702	IN1703	IN1704	IN1706	IN1707	IN1708
		P	P	P	M	S	S
	Temperature (°C)	68	15	15	82.6	92.1	44
Misc. Phases	Am. Silica	+				XXX	
	Anatase					X	
	Kaolinite						X
	Sulfur				XXX		
Carbonates	Aragonite	XXX	XXX	XXX			
	Calcite	X	X	X			
Fe-sulfides	Pyrite				+		
Ca-sulfates	Gypsum				+		

Table 4- Minerals forming in a neutral hot spring and an acidic mud pot two drainages to the south of the red and white river confluence. Samples collected in and near the neutral hot spring are indicated in gold, while samples collected in and near the acidic mud pot are indicated in blue. S- soil, P- precipitate, M- mud. XXX- abundant, XX- common, X- present, +- rare.

Mineral assemblages in and near the travertine-precipitating hot spring (pH 7.49), as well as an acidic mud pot nearby, are presented in Table 4. The canal walls bounding the neutral hot spring runoff are primarily aragonite and some calcite (IN1702), with a trace amount of amorphous silica (Figure 9). The fossil deposits located around the spring (IN1703 and IN1704) are of the same composition as the canal walls but have no trace of amorphous silica. A nearby

acidic mud pot (pH 2.92) has sulfur-rich mud with trace amounts of pyrite and gypsum. The surrounding leached soil is rich in residual minerals. The XRD pattern of the red-orange soil (IN1708) around the pool has a high background and a small amount of kaolinite. The largely X-ray amorphous nature of the sample (coupled with high background) and high Fe_2O_{3T} concentration determined by XRF suggests iron fluorescence during XRD analysis and the likely presence of a nanophase Fe oxide or hydroxide.

Hveragerdi neutral hot spring

		IH1311	IH1313	IH1314	IH1702
		P	S	P	P
	Temperature (°C)	90	90	10.3	71.4
Misc. Phases	Amorphous silica	XXX	XXX	XXX	
	Calcite			XX	
	Halite			X	
	Kaolinite		X		
	Sulfur				XXX
Fe-Sulfide	Pyrite				+
Ca-Sulfate	Gypsum				+

Table 5- Minerals forming in a neutral hot spring. S- soil, P- precipitate. XXX- abundant, XX- common, X- present, +- rare.

Mineral assemblages (Table 5) from a neutral hot spring in the Hveragerdi geothermal field (pH 8.3) were sampled in 2013 and 2017. Layered precipitate deposits sampled near the hot spring (IH1311) are composed of amorphous silica. The layered deposits composing the walls of the hydrothermal pool are of the same composition as these layered deposits, but also contain some kaolinite. A stream discharge downhill from the hot spring was precipitating a fibrous coating (IH1314) composed primarily of amorphous silica with some calcite and halite. Three years later, the neutral hot spring was a bubbling pool buried under a small rock pile. White and

yellow precipitates on the overhang of the wall (IH1702) are primarily sulfur with trace amounts of pyrite and gypsum.

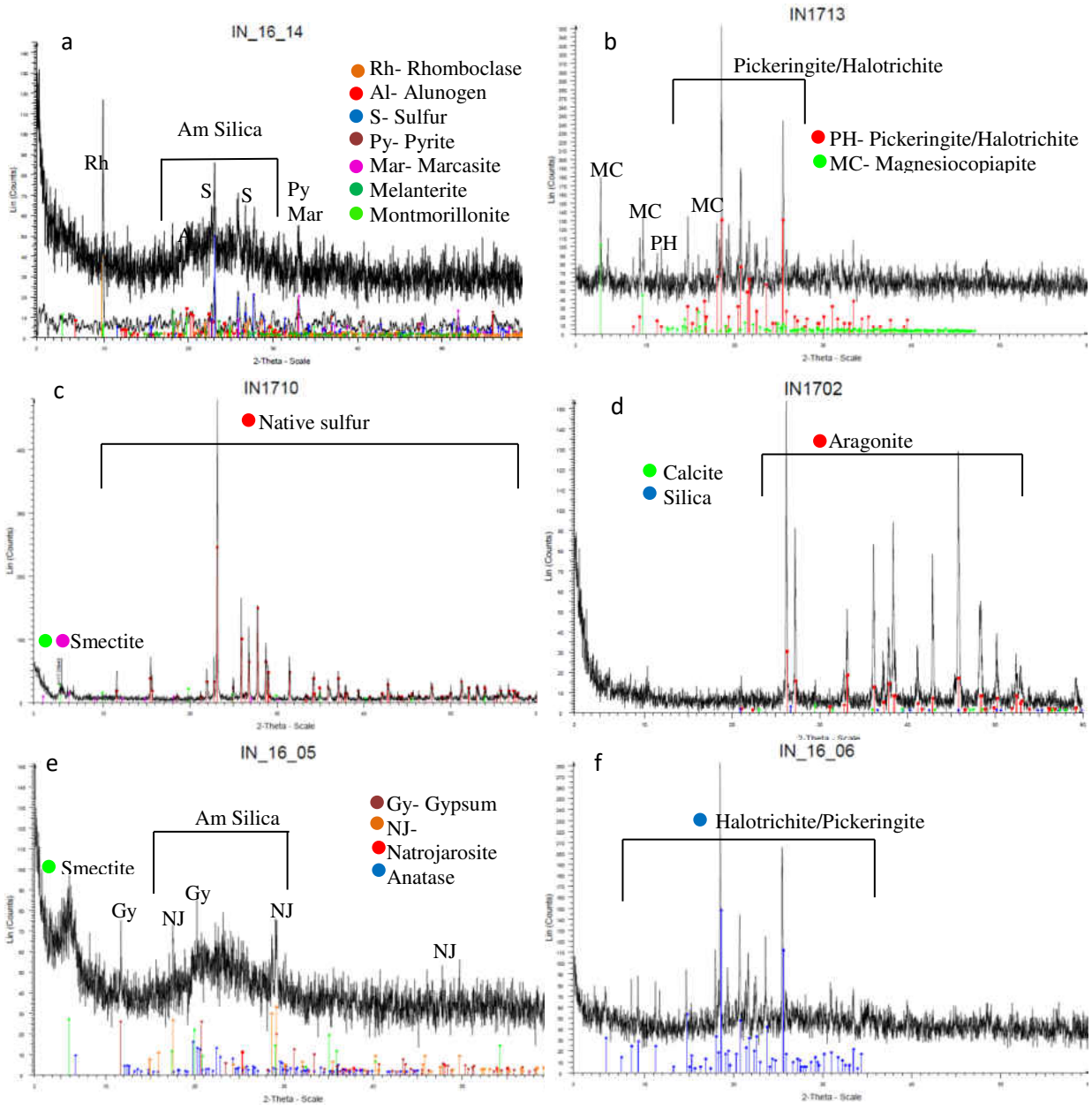

Figure 11- Representative XRD patterns around the two hydrothermal streams, the near neutral springs, and the neutral spring in the Nesjavellir geothermal field. Significant peaks are labeled with the mineral. a) Precipitated crust on the margin of an acidic spring pouring into the red stream. b) Crinkly precipitate on the steam-heated bank of the white stream. c) The white precipitate characteristic of the white stream. d) Canal walls in travertine-depositing neutral hot spring. e) Orange, crinkly precipitate near the northern near-neutral hot spring. f) White, cauliflower-like precipitate near IN1605.

4.2 XRF

	Near-neutral spring				Red stream			Substrate	Mud pots		Sinter spring		
Sample	IN1603	IN1604	IN1605	IN1607	IN1611	IN1612	IN1614	IN1616	IN1708	IN1718	IH1311	IH1313	IH1314
SiO_2	90.75	37.98	43.96	31.99	23.53	38.61	55.47	47.45	47.00	32.48	89.86	86.41	86.41
TiO_2	3.85	2.23	1.60	2.04	0.06	1.71	1.80	2.20	5.98	2.49	0.10	0.35	0.35
Al_2O_3	1.37	13.38	9.37	12.87	3.83	24.18	8.52	14.76	4.62	15.35	1.59	3.39	3.39
Fe_2O_3	0.49	29.52	12.20	20.43	54.15	13.32	9.08	13.15	32.50	12.71	0.83	1.41	1.41
MnO	ND	0.04	0.07	0.13	ND	0.01	0.02	0.20	0.03	0.03	0.00	0.01	0.01
MgO	0.22	2.13	2.63	1.37	0.34	0.68	1.20	6.48	0.60	1.00	0.22	0.26	0.26
CaO	0.09	0.63	3.05	0.99	0.10	0.04	1.06	12.20	0.28	0.71	0.66	0.50	0.50
Na_2O	ND	0.05	0.77	0.15	ND	ND	0.02	1.97	ND	0.04	0.24	0.22	0.22
K_2O	0.14	0.03	0.14	0.03	0.02	ND	0.14	0.19	0.07	0.04	0.14	0.08	0.08
P_2O_5	0.10	0.24	0.13	0.14	1.13	0.13	0.17	0.25	0.79	0.29	ND	0.02	0.02
LOI	5.28	11.00	17.30	23.80	13.60	15.40	18.60	-0.49	7.06	34.50	0.74	0.66	1.04
Sum	102.24	97.35	91.32	93.96	97.63	94.25	96.19	98.99	99.30	99.81	92.89	92.06	91.82

Table 6- Major and minor element compositions of samples collected from the Nesjavellir geothermal field, presented as weight percentages (wt%). 'ND' represents elements not detectable in the sample. Light blue is the northern near-neutral spring, red is the acidic red stream, gray is the substrate, dark blue is the acidic mud pot near the neutral spring, the dark red is the acidic mud pot uphill from the red stream, and the bright green indicates the sinter-depositing neutral spring in the Hveragerdi geothermal field.

XRF results for major and minor elements are presented in Table 6, and trace element compositions are presented in Table 7. Spidergram plots, in which select samples are normalized against the unaltered substrate, are presented in Figure 12, bivariate plots are presented in Figure 13, and isocon plots are presented in Figure 14. Relative depletions of MnO, MgO, CaO, Na_2O, K_2O (and to a lesser degree P_2O_5) are observed for most of the altered rock, soil, and mud

	Near-neutral spring				Red stream			Substrate	Mud pots		Sinter spring	
Sample	IN1603	IN1604	IN1605	IN1607	IN1611	IN1612	IN1614	IN1616	IN1708	IN1718	IH1311	IH1313
Y	ND	ND	ND	ND	ND	ND	47	ND	ND	ND	ND	ND
Zr	161	107	82	103	ND	68	82	112	290	111	ND	ND
Nb	ND	ND	ND	18	ND	ND	ND	ND	51	ND	ND	ND
V	128	608	457	336	2439	442	310	362	2665	644	ND	54
Zn	ND	62	ND	115	ND	218	63	113	ND	215	ND	ND
Ni	ND	64	ND	158	96	428	162	87	57	127	ND	ND
Cr	258	416	242	293	368	313	217	255	450	263	ND	ND
Ce	30	27	26	20	19	18	25	20	36	25	ND	ND
Sr	ND	ND	55	ND	ND	ND	148	249	ND	45	43	63
Ba	ND	ND	ND	ND	ND	ND	101	ND	146	ND	ND	ND

Table 7- Trace element compositions of samples collected from the Nesjavellir geothermal field in parts per million (ppm). 'ND' represents elements not detectable in the sample. Light blue is the northern near-neutral spring, red is the acidic red stream, gray is the substrate, dark blue is the acidic mud pot near the neutral spring, the dark red is the acidic mud pot uphill from the red stream, and the bright green indicates the sinter-depositing neutral spring in the Hveragerdi geothermal field.

samples. Al_2O_3 enrichments occur in deposits rich in clay minerals, such as IN1612 (24.18 wt% vs. 14.76 wt%). The XRD patterns for samples IN1611 and IN1708 have high backgrounds and are largely X-ray amorphous. The two are also highly enriched in Fe_2O_3 (54.15 wt% and 32.50 wt%, respectively) (Figure 13) indicating likely iron fluorescence in the XRD analyses. IN1604 (orange coating) and IN1607 (dark grey mud at a few cm depth) also have elevated Fe_2O_3 concentrations of 29.52 wt% and 20.43 wt% (Figure 12). High concentrations of SiO_2 are observed in the leached rock from the northern spring (IN1603 at 90.75 wt%) (Figure 14a) and samples from the Hveragerdi sinter spring (IH1311 at 88.45 wt%, IH1313 at 85.19 wt%, and IH1314 at 86.61 wt%). Higher TiO_2 concentrations relative to the substrate occur in IN1603 (3.85 wt% vs. 2.20 wt%), IN1708 (5.98 wt% vs. 2.20 w%), and to a lesser degree in IN1718 (2.49 wt% vs. 2.20 wt%) (Figure 13). General depletion is observed for MgO, with the substrate concentration at 6.48 wt% and all other samples below 3.00 wt% (Figure 13b). The same general

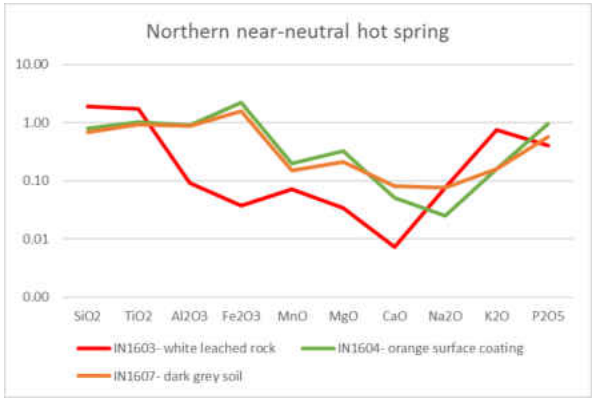

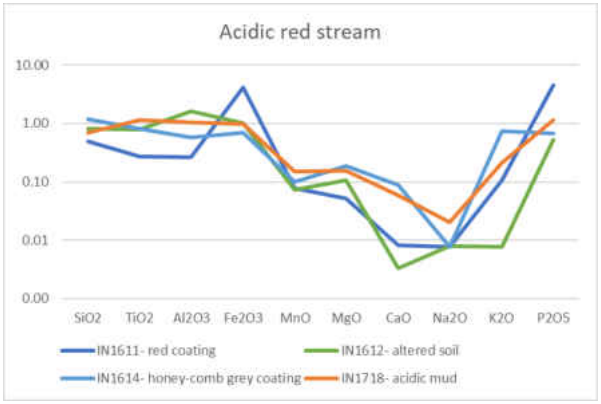

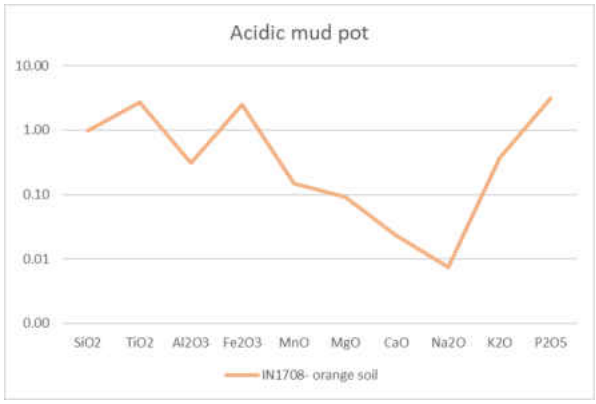

Figure 12- Major element compositions of samples collected from the Nesjavellir geothermal field, normalized to the unaltered substrate and plotted as spidergrams showing enrichment or depletion of soil and mud samples. For elements not reported because their concentrations were less than 2 times the lower limit of detection, the lower limit of detection was plotted for the spidergrams. Overall leaching of the mobile cations can be seen across the geothermal field.

trend can be observed with CaO, with the substrate at 12.02 wt% and the altered products at less than 2.00 wt% (Figure 13f). High P_2O_5 concentrations relative to the substrate are observed in

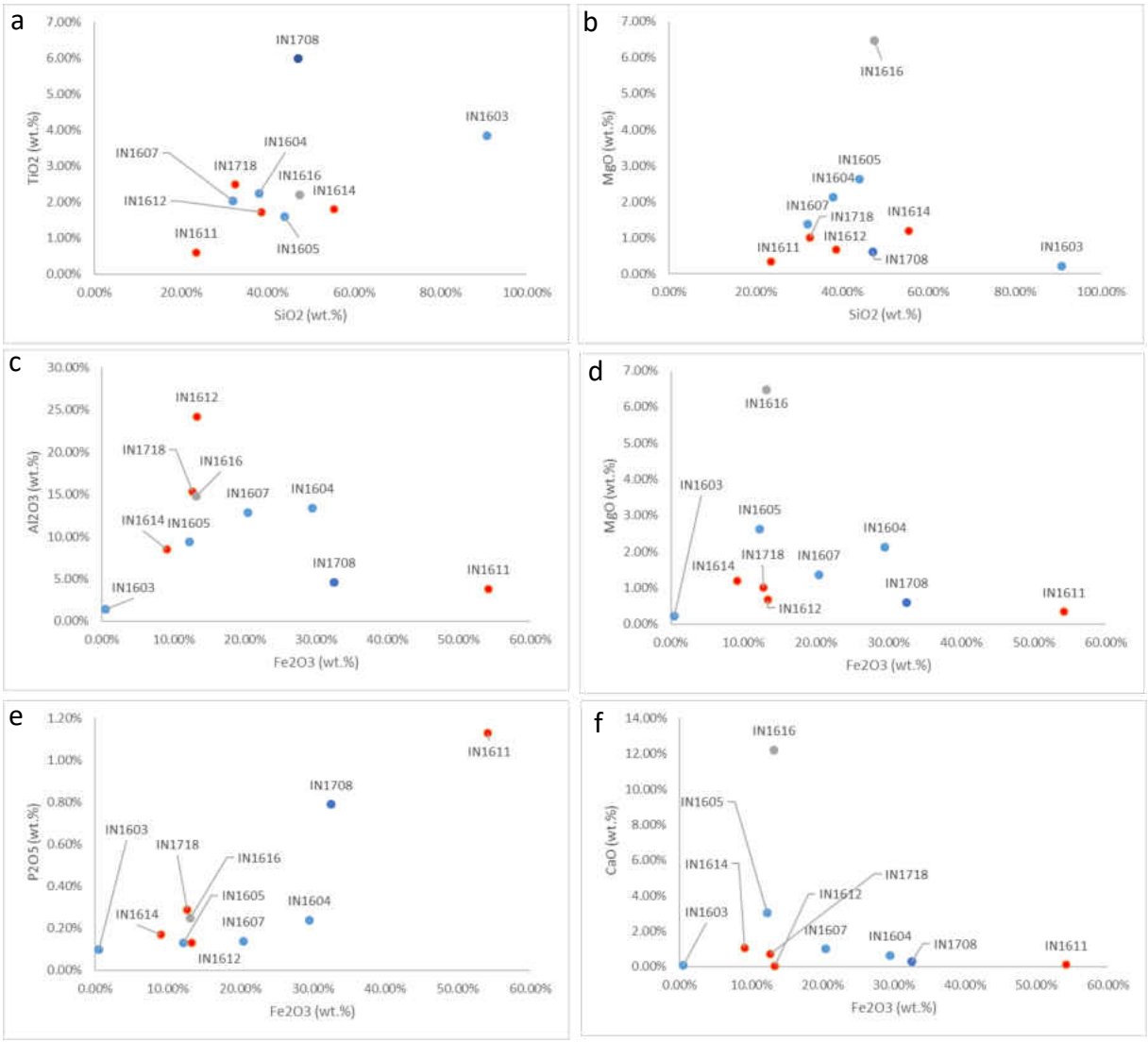

Figure 13- Bivariate plots of samples analyzed by XRF. Red- acidic stream, blue- northern spring, dark blue- acidic mud pot near travertine, grey- substrate. a) SiO_2 vs. TiO_2. b) SiO_2 vs. MgO. c) Fe_2O_3 vs. Al_2O_3. d) Fe_2O_3 vs. MgO. e) P_2O_5 vs. Fe_2O_3. f) Fe_2O_3 vs. CaO. The substrate (IN1616) has higher concentrations of CaO and MgO than altered precipitates. Leached soil samples IN1708 and IN1603 have higher SiO_2 and TiO_2 than the substrate, due to residual enrichment. However, sample IN1614 has a higher silica content than the substrate, but less TiO_2, consistent with precipitation of silica. Clay rich soil IN1612 has higher concentrations of Al_2O_3 than other altered products and substrate. P_2O_5 is enriched in deposits with higher Fe_2O_3 concentrations.

the iron fluorescent samples IN1611 (1.13 wt% vs. 0.25 wt%) and IN1708 (0.79 wt% vs. 0.25 wt%) (Figure 13e).

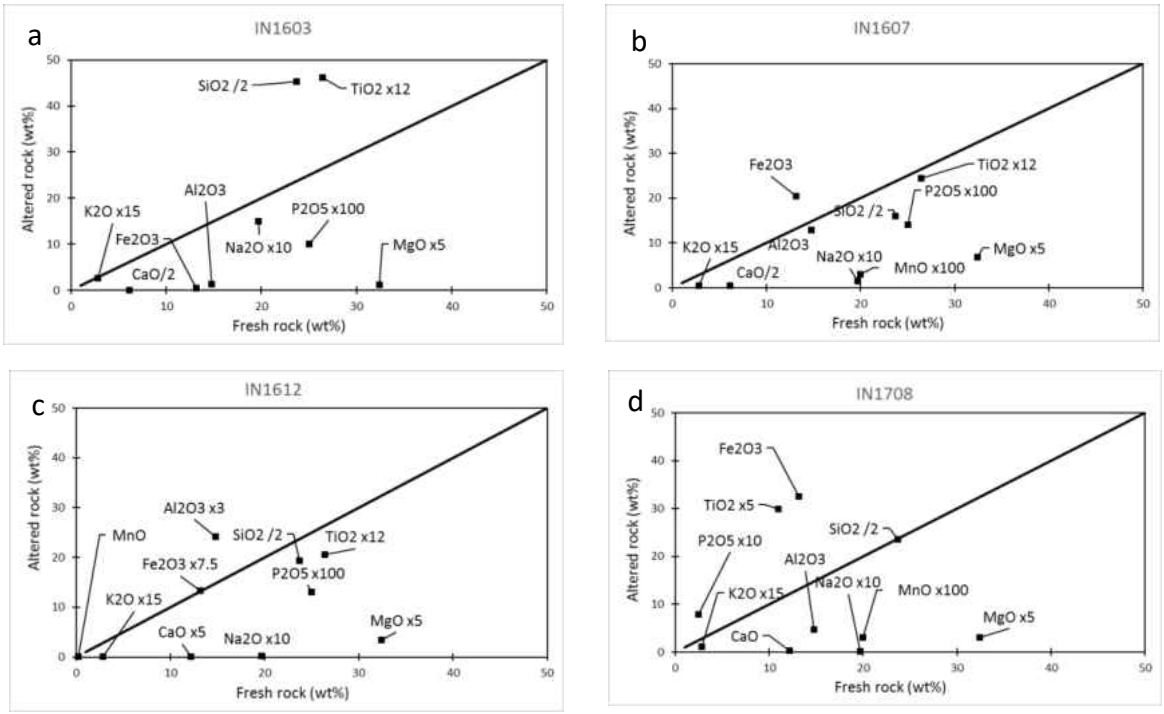

Figure 14- Isocon plots of altered soils analyzed by XRF. These plots show the enrichment of major and minor elements relative to a sample of less altered substrate. The concentrations for both the substrate and altered sample were arbitrarily multiplied or divided by a number to allow all major and minor elements to be plotted together. The line in the center of the plots is a 1:1 line, above which indicates enrichment and below which indicates depletion of a given element. a) IN1603 is the leached white rock from the northern spring, and shows enrichment of SiO_2 and TiO_2 and depletions of more mobile cations. b) IN1607 is the dark grey soil at few cm depth near the northern spring, and shows Fe_2O_3 enrichment, while other major cations are substantially depleted, except for Al_2O_3, which is only slightly depleted. c) IN1612 is the clay-rich embankment being cut into by the red stream, and shows enrichment in Al_2O_3. Fe_2O_3 content is comparable to substrate levels. d) IN1708 is the orange, patchy soil from the acidic mud pot near the travertine spring, and exhibits high Fe_2O_3 concentrations with respect to the substrate. TiO_2 and P_2O_5 are enriched, and SiO_2 concentrations are comparable to the substrate.

4.3 Aqueous Geochemistry

Site	Sample	T (*C)	pH	ORP (mV)	Salinity (psu)	DO (mg/L)	Cond. (µS/cm)	Spec. Cond. (mS/cm)	TDS (g/L)
Neutral spring	IN1701	68.0	7.49	237.51	0.31	3.11	923.51	0.61	0.39
	IN1705	82.6	2.92	565.44	0.59	1.84	1568.73	1.17	0.75
Northern	IN1601	81.8	5.60	NA	0.18	NA	497.35	0.37	0.24
Acidic and near neutral streams	IN1608	22.9	5.65	NA	0.08	NA	141.02	0.16	0.10
	IN1711	10.2	5.82	96.64	0.06	9.78	87.66	0.12	0.08
	IN1712	15.1	6.19	119.58	0.17	9.37	288.28	0.35	0.22
	IN1714	4.8	6.20	217.37	0.06	11.60	88.49	0.13	0.08
	IN1709	81.7	5.79	24.93	0.07	0.51	190.57	0.14	0.09
	IN1610	63.5	3.19	NA	0.30	NA	788.39	0.61	0.39
	IN1716	64.7	3.82	258.13	0.14	2.91	391.05	0.28	0.18
	IN1613	93.2	2.28	NA	1.65	NA	4108.40	3.15	2.02
	IN1717	94.9	2.58	358.83	1.20	2.12	2120.26	2.33	1.49
	IN1615	21.3	6.53	NA	0.08	NA	155.96	0.17	0.17
	IN1715	24.2	6.13	102.61	0.08	6.88	181.20	0.16	0.10
Sinter	IH1701	99.3	8.30	52.94	0.20	0.00	624.32	0.40	0.26

Table 8- Hydrolab results for the Nesjavellir geothermal field. Orange: travertine-precipitating neutral hot spring, light blue: various hot springs, yellow: near-neutral white stream, red: acidic red stream, green: confluence of the two streams, bright green: sinter spring in the Hveragerdi geothermal field.

The Hydrolab results (Table 8) show that low pH is associated with high oxidation-reduction potential (ORP) across the different hydrothermal features (Figure 15). More acidic hydrothermal features are typically associated with highly oxidizing conditions, while near-neutral features are more often associated with reducing environments. There are exceptions to this; for example, the neutral travertine-depositing spring has a higher ORP very similar to more acidic features. This neutral, travertine-depositing spring actually shares many characteristics with the more acidic springs, including higher salinity, conductivity, and total dissolved solids (TDS) than other near-neutral sites. The near-neutral spring north of the two streams (IN1601) also shares this similarity with more acidic features. 2017 measurements of the Hveragerdi sinter spring (IH1701) show an alkaline pH with a low ORP. The near-neutral white stream has varying environmental conditions as the stream travels downhill, with ORP decreasing down slope while

the conductivity increases. The water sampled at the confluence of the red and white streams has similar environmental conditions to the white stream, as expected since the white stream has a greater volume. 2017 field work occurred at a different time of year (early July, as opposed to late August/ early September), which revealed that there is likely some seasonal or year to year variation in the conditions of these systems.

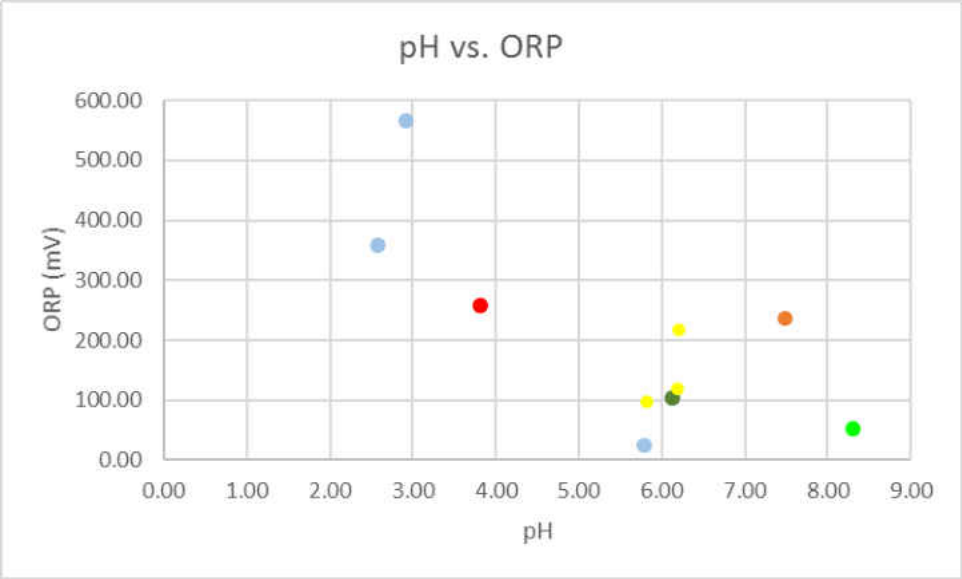

Figure 15- Plot of pH vs. ORP (in mV). Orange: travertine-precipitating neutral hot spring, light blue: various hot springs and mud pots, yellow: near-neutral white stream, red: acidic red stream, green: confluence of the two streams, bright green: sinter spring in the Hveragerdi geothermal field. Conditions become less oxidizing with increasing pH.

Site	Sample	K	Na	Mg	Ca	Fe2+	HCO3-	Cl-	SO4
Neutral spring	IN1701	12.93	71.06	12.09	55.99	0.10	288.36	11.75	ND
	IN1705	6.54	6.55	14.94	23.01	7.00	188.55	10.91	89.54
Acidic and near neutral streams	IN1608	0.47	7.14	0.23	2.68	NA	NA	12.71	0.00
	IN1711	5.16	8.57	2.61	9.88	0.00	38.82	11.75	14.43
	IN1712	5.51	8.57	2.77	9.92	0.00	44.36	11.69	14.81
	IN1714	5.75	1.24	0.25	14.29	0.00	44.36	11.72	13.38
	IN1709	4.59	7.96	2.29	9.13	0.00	27.73	11.72	15.27
	IN1610	0.36	6.79	10.76	10.77	NA	NA	12.50	96.56
	IN1716	3.14	10.11	6.10	11.30	1.50	*55.11	11.68	33.11
	IN1613	0.59	4.85	65.79	45.98	NA	NA	11.84	592.40
	IN1717	8.19	7.75	18.31	19.48	50.00	*212.50	13.80	171.49
	IN1715	6.83	8.50	3.97	10.42	1.00	*43.05	11.67	18.87
Sinter	IH1701	13.59	84.76	ND	2.16	0.00	83.18	12.81	21.64

Table 9- Major anion and cations in the hydrothermal waters, in mg/L. ND- Not detectable, NA- not analyzed. Values with an asterisk were calculated from the sample's molar equivalence rather than measured, assuming the samples were electrically balanced. The results are color coordinated according to the scheme used in Table 7.

The AA and IC results (Table 9) show higher SO_4^{2-} concentrations in acidic hydrothermal waters than in neutral and near-neutral hydrothermal waters. Cl^- concentrations, by contrast, remain relatively constant throughout the Nesjavellir geothermal field, regardless of acidity (Figure 16). Water from the travertine-forming neutral hot spring has high concentrations of Na^+,

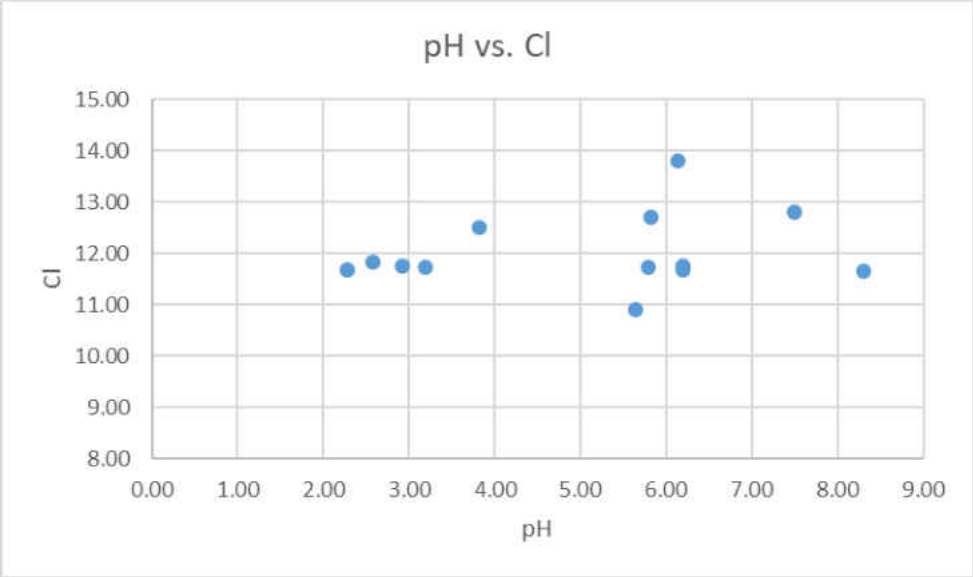

Figure 16- Plot of pH vs. Cl^-. Cl^- is in mg/L. Cl- concentrations remain relatively constant across all environments, ranging from acidic to alkaline.

Ca^{2+}, and bicarbonate, which is consistent with travertine precipitation. Acidic hydrothermal features have a higher concentration of Fe^{2+}, bicarbonate, and SO_4^{2-} than the more neutral sites. The alkaline sinter spring at the Hveragerdi geothermal field contains more K^+ and Na^+ than the hydrothermal systems at Nesjavellir and has a Cl^- concentration similar to Nesjavellir.

4.4 SEM/EDS

Several pieces of the canal wall from the travertine-forming neutral hot spring were analyzed by SEM to examine any biogenic content. Well-formed aragonite crystals, pseudobiogenic structures and amorphous concretions, and a variety of potential biological structures were observed throughout the sample (Figure 17). Long, slender prismatic crystals of aragonite are the major constituent and are present throughout the sample and are assumed to be

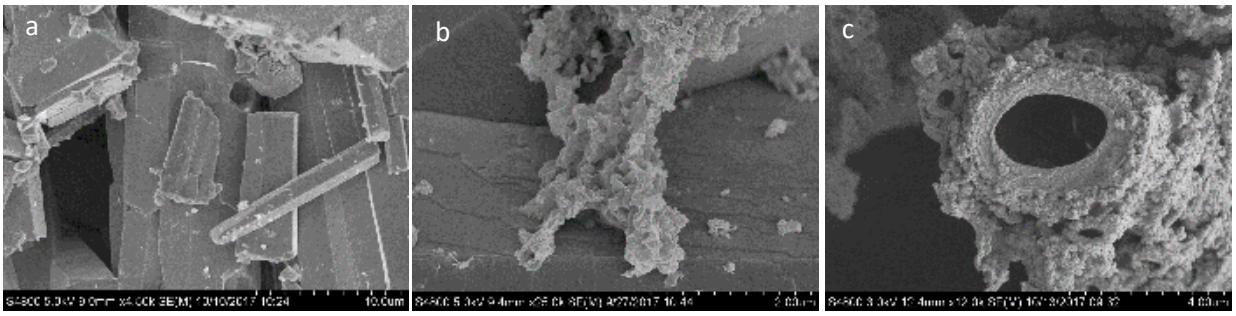

Figure 17- Various structures observed in the canal wall. a) Aragonite crystal clusters make up most of the sample. b) Globules of aragonite/silica form and adhere to different surfaces and form various structures. c) Microtubules, while rare, are found in certain areas of the sample.

abiogenic. Potentially biogenic features, such as microtubules, microsheaths, and other possible biological structures (Geptner et al., 2005), are abundant in specific areas only. Typically, abiogenic and biogenic features are present near each other in select areas of the sample. These abiogenic features often appear strikingly similar to biogenic features.

Aragonite

The slender, prismatic (acicular) crystals that make up most of the sample are usually present in clusters, growing parallel to each other as semi-botryoidal growths (Figure 15a). These crystals also occasionally exhibit stellate structures, with a point of nucleation and several crystals radiating out from the center (Figure 18). The mineral is identified as the calcium carbonate mineral aragonite based on its XRD pattern, which is consistent with the EDS results showing a combination of calcium, carbon, and oxygen.

Figure 18- Prismatic aragonite crystals radiating out in a stellate habit.

Pseudobiological abiogenic structures

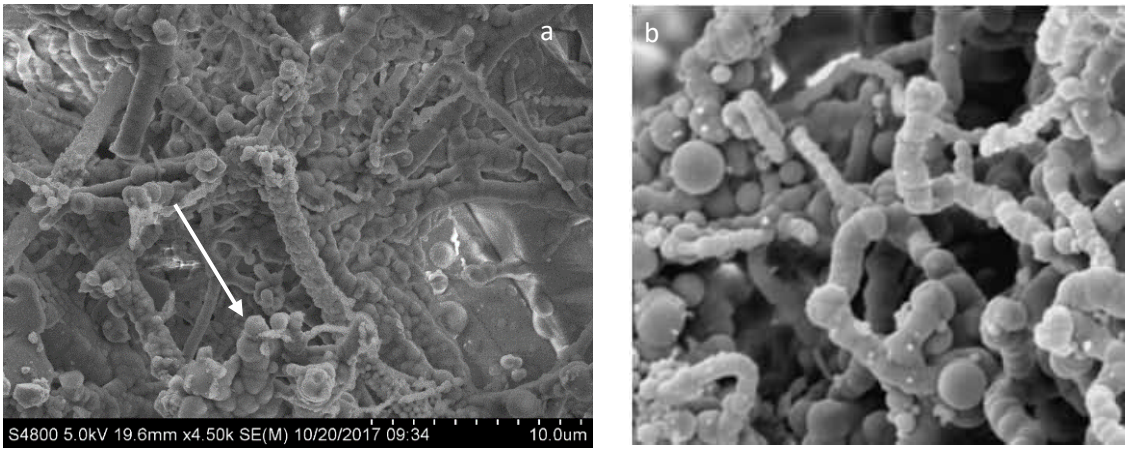

Figure 19- a) Abiogenic concretions forming tubes and filaments in sample IN1702. Arrow pointing to an amorphous concretion. b) Merging silica globules formed from hydrological processes presented in Geptner et al. (2005).

Pseudobiogenic structures are common throughout the sample and are typically composed of a mixture of silica and aragonite, although some are pure silica. These abiogenic structures occur as amorphous concretions, tubular structures, and massive surfaces. While all of these structures are reminiscent of biological features, the presence of merged globules suggests that these various tubes and filaments are the result of abiogenic processes (Geptner et al., 2005)(Figure 19).

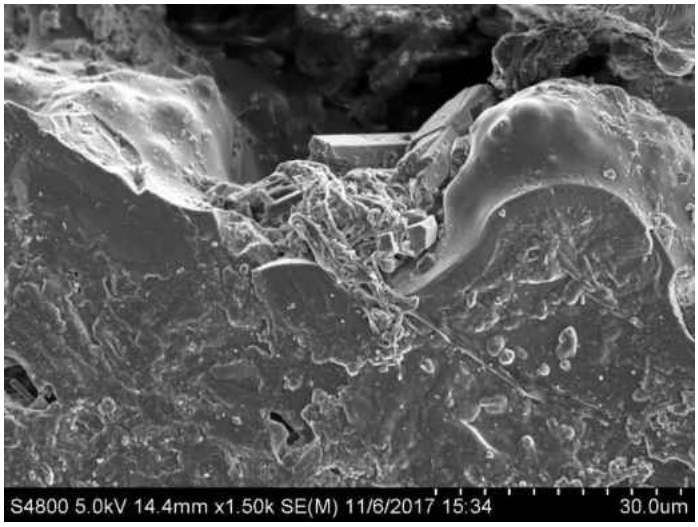

Figure 20- Massive amorphous surface in the canal walls.

Amorphous concretions are ubiquitous throughout the sample, and are often found as globules adhering to crystals, biological structures, and to each other. When the globules form,

they can adhere to one another to form tubular structures that resemble biological features. Large, massive amorphous surfaces are found in the sample material and can preserve unique features. The massive amorphous surfaces, while similar to some of the amorphous concretions, a difference in composition shows that they likely did not form from similar processes (Figure 20). EDS analysis of the small globules show a mixture of carbonate and silica, but the abiogenic tubes and massive surfaces are almost pure silica.

Biological structures

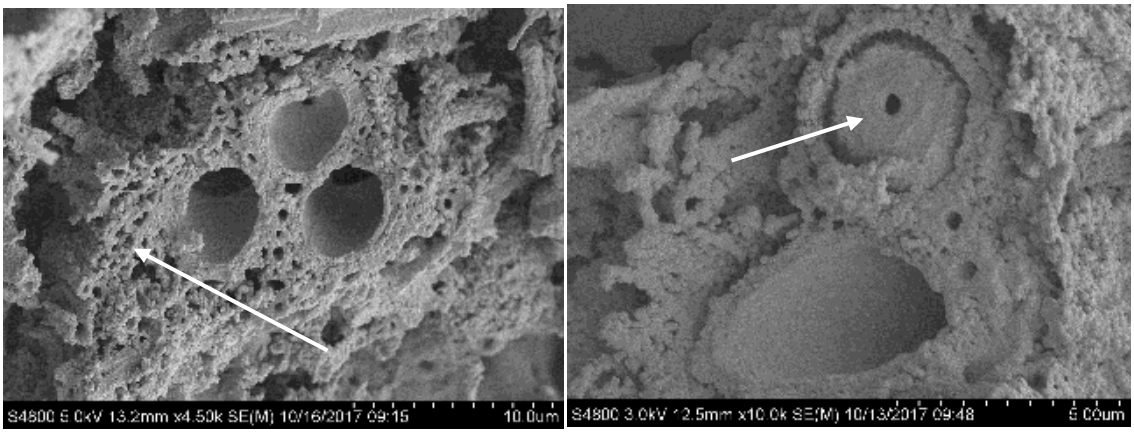

Figure 21- Biologically mediated tubes. a) Three tubes which seem to be glued together by a network of smaller, abiological tubes indicated by an arrow. They appear to have rims and a concave feature inside. b) An unknown, possibly biological feature (indicated by an arrow) inside a tube.

Biological structures are typically restricted to certain areas of the sample and are composed of silica globules. However, the silica globules on these structures typically occur only on the outside of the tube, while the interior of the tube is relatively smooth (Figure 21a). These tubes vary in size from 2 to 5 microns. The interiors of some tubes also contain structures, occasionally with rims, or more rarely an unknown, possibly biological structure filling an entire microtubule, which often appears with a hole at the very center (Figure 21b). This feature appears to be made mostly of silica globules, but the side is flat with a hole in the middle. This feature occurs rarely, and only inside these tubules. Possible abiogenic tubes also form with these

biological tubes and are much smaller. These smaller tubes are irregular, forming mostly from globules that randomly adhere (Figure 19a).

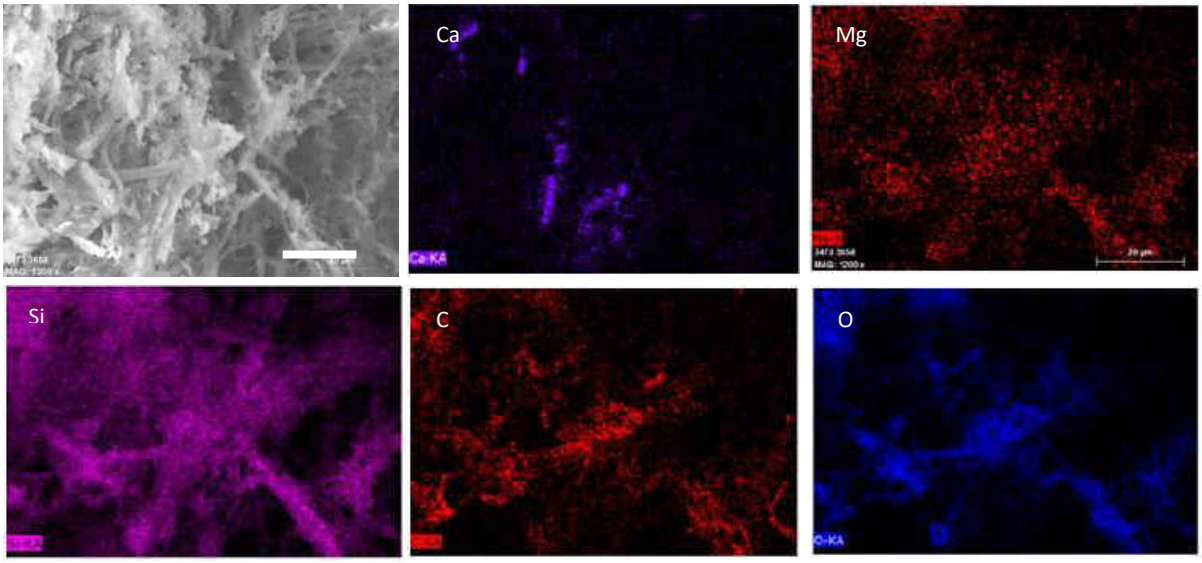

Figure 22- EDS analysis of fuzzy green filaments. These filaments are rich in silicon, supporting the idea that these could be diatoms. White bar is 20 microns, and the magnification is 1,200x.

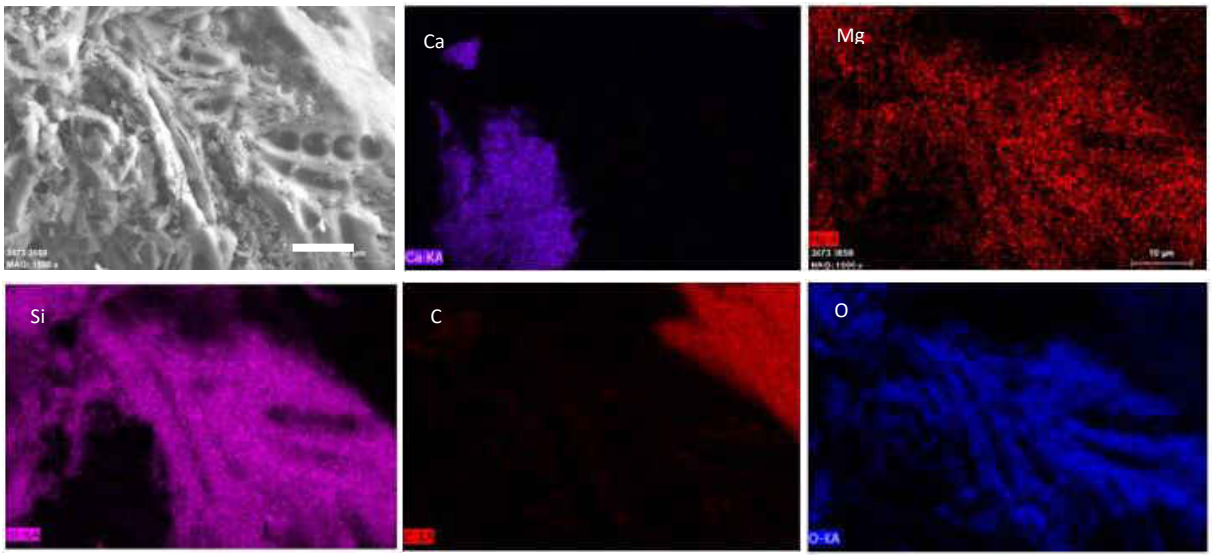

Figure 23- EDS element maps of the edge of the canal wall, with unusual supposed biological structures preserved. The biological features are located in areas composed of almost pure silicon and oxygen but have a faint magnesium signature. The magnification is 1,500x, and the white bar is 10 microns.

Biological structures also occur as fuzzy green filaments, which resemble an assortment of centric diatoms (Heather Owen, pers. comm.). Several unusual shapes, such as "pea-pod" shapes and possible cross sections of the microtubes occur in the massive amorphous surfaces. EDS analysis of the green filaments (Figure 22) and the biological structures in the precipitate (Figure 23) reveal that both are made up of silica, with little trace of calcium in the silica-rich regions. Magnesium is also elevated in the silica-rich portions.

5. Discussion

5.1 Occurrence of hydrothermal products and their environments

The minerals produced by the processes altering the basaltic substrate are heavily influenced by the environment in which they are formed. Sulfates can often be found as precipitates or as part of mud in highly oxidizing, acidic hydrothermal environments. Fe-bearing sulfates occur most often, followed by Al-sulfates, and can be found in association with acidic mud pots in both precipitates and acid mud. The prevalence of Fe-bearing sulfates is partially attributed to the Fe-rich nature of Mt. Hengill's tholeiitic basalt. Several sulfate precipitate samples (IN1605, IN1606, and IN1713) had formed close to near-neutral environments, although these precipitates are not the result of these environments. Subtle, disseminated fumarolic activity likely formed these precipitates, as the precipitates often occur on surfaces hotter than the surrounding area. Fe- and Al-bearing sulfate phases are common throughout Nesjavellir, with Mg- and Ca-sulfates occurring rarely.

Fe-sulfides and native sulfur are often found as precipitates and as constituents of hydrothermal mud and are present throughout the various sites of the Nesjavellir geothermal field, regardless of the hydrothermal environment. The Fe-sulfides and native sulfur commonly

occur with sulfates in acidic, oxidizing environments. A notable exception is the white stream, where native sulfur and some montmorillonite precipitate out of the near-neutral stream (Figure

Figure 24- The Hveragerdi sinter pool. Much of it is covered by large rocks, some of which were removed to sample the water (pH 7.7, IH1701). The yellow precipitate forming above the sinter pool is IH1702. Jacob staff for scale.

10d). The Fe-sulfides detected in precipitates and muds are usually present in small amounts. This oxidizing environment could be a recent feature of the hydrothermal system or is (more likely) constrained to surface waters with more reducing conditions at depth, which could explain the presence of sulfide minerals more consistent with a reducing environment. The sulfur precipitate in the Hveragerdi sinter spring is formed primarily by fumarolic activity, with much of the precipitate forming above the sinter pool (Figure 24).

The residual phases anatase, amorphous silica, and various clay phases are found in areas of high hydrothermal activity, and often indicate intense leaching. The northern near-neutral spring has the high-temperature silica phase tridymite, a possible remnant from a previous high-temperature regime. Several localities in the geothermal fields have abundant amorphous silica

but lack anatase, which is reflected in the XRF results with higher concentrations of SiO_2 than the substrate (55.47 wt% for IN1614 and >85 wt% for samples from Hveragerdi vs. 47.45 wt% for the substrate) but have only minor amounts of TiO_2 (1.8 wt% and <0.40 wt% vs. 2.20 wt%) (Figure 13a). The northern spring also has a high SiO_2 content (90.75 wt%) but the TiO_2 content is also elevated (3.85 wt%), and the residual phase anatase is present (Figure 14a). The lack of TiO_2, a relatively immobile cation, at areas of silica enrichment suggests that the silica is not residual, but rather precipitated by the hydrothermal fluid. A thin, amorphous silica rich crust (IN1614) is observed adjacent to the acidic spring near the red stream (IN1613). The alkaline Hveragerdi spring (IH1701 and IH1311, 13, and 14) also precipitated silica sinter, which formed layered sinter deposits near the spring. These layered deposits are similar to the layered deposits comprising the pool walls, which suggests a common origin. These deposits formed in low-ORP alkaline waters.

The travertine forming in the neutral hot spring is aragonitic with some calcite and formed in an oxidizing environment (ORP 237.51 mV). The formation of travertine is a long-standing feature of this spring, with abundant fossil travertine deposits throughout the immediate area. The fresh travertine has a small amount of siliceous material, which preserves biogenic features. Numerous microtubes, microsheaths, and unusual microstructures are preserved by silica, rather than aragonite or calcite. These structures could have been silicified by microbial processes that would have led to the deposition and formation of silica, preserving evidence for the biological activity (Konhauser et al., 2001). However, they could also have just been preserved by the abiogenic process of silica deposition induced by temperature changes, solution mixing, evaporation, release of steam phases, or a change in pH (Geptner et al., 2005).

Figure 25- Red biofilm of the acidic stream (sample IN1610 and IN1611, water and precipitate respectively). Jacob staff for scale (gradations are 10 cm).

The red biofilm characteristic of the acidic red stream is X-ray amorphous, has a high background in its XRD pattern, and is primarily composed of iron (54.15 wt% Fe_2O_3T), which suggests the occurrence of nanophase Fe-oxides or hydroxides (Figure 25). The nanophase oxides and/or hydroxides occur in oxidizing (ORP 258.17 mV), acidic (pH 3.82) conditions, and were likely formed by biological activity.

5.2 Mobility, transport, and occurrence of elements

In altered products, relative depletion of MnO, MgO, CaO, Na_2O, K_2O, and to a lesser degree P_2O_5 is widespread throughout Nesjavellir, while Fe_2O_3 and Al_2O_3 can be enriched or depleted, depending on the intensity of alteration (Figures 12, 13, and 14). Higher Fe_2O_3 and Al_2O_3 concentrations can be found in precipitates, while high Fe_2O_3 concentrations are noted in samples that have XRD patterns with high backgrounds and few diffraction peaks, suggesting the presence of X-ray amorphous nanophase Fe-oxides at multiple sites throughout Nesjavellir

(Figure 13). High Fe_2O_3 concentrations can also occur at sites rich in Fe-sulfides, as is the case for sample IN1607 from the northern spring (Figure 14). Figure 13c shows Al_2O_3 enrichments occur in two samples composed of clay minerals and a variety of sulfates, which include Al-rich sulfates. Al_2O_3 concentrations are lower in most of the samples compared to the substrate as shown in both Figure 13 and 14, but to a lesser extent than other mobile cations. Higher concentrations of SiO_2 and TiO_2 can co-occur in extensively leached samples, such as IN1603 (90.75 wt% and 3.85 wt%, respectively). The isocon plots of Figure 14 show high relative enrichment of SiO_2 and TiO_2 compared to the less altered substrate in IN1603, and show enrichment of Al_2O_3 in sample IN1612, the altered bank of the red stream. These elements are relatively immobile compared with other cations and are thus concentrated in the residue left by acid-sulfate leaching. However, sample IN1614 from the mud pot near the red stream has slightly elevated SiO_2 and slightly depleted TiO_2, along with abundant amorphous silica identified by XRD. It is therefore likely that this SiO_2 enrichment is tied to silica precipitation rather than acid-sulfate leaching. The isocon plots in Figure 14 show general depletion of mobile cations, with the exceptions of Fe_2O_3, Al_2O_3, and P_2O_5. The abundant Fe_2O_3 present in IN1607 is likely due to the Fe-sulfides and remnant material present in the soil, while the Fe_2O_3 present in IN1708 is due to the nanophase Fe-oxides. The Al_2O_3 enrichment occurring in the bank of the red stream (IN1612) is likely due to the abundant clays present in the bank. The enrichment in P_2O_5 in IN1708 shown by the isocon plots is unusual, but also occurs in the red biofilm (IN1611).

XRF results for the soils, altered rocks, and mud samples show that the more mobile cations are generally depleted compared to those from the substrate. These cations were likely leached from the basalt by acidic hydrothermal fluid, and then mobilized out of the hydrothermal

system. This can be seen in water collected from acid mud pots IN1705, IN1613, and IN1717, where acidic and oxidizing conditions are dominant. The water sampled at these mud pots had higher concentrations of Fe^{2+}, Mg^{2+} and Ca^{2+} than more neutral hydrothermal waters, such as IN1709 or IH1701. Ternary diagrams plotting cations (Mg^{+}, Ca^{+}, $Na^{+}+K^{+}$) and anions (SO_4^{2-}, Cl^{-}

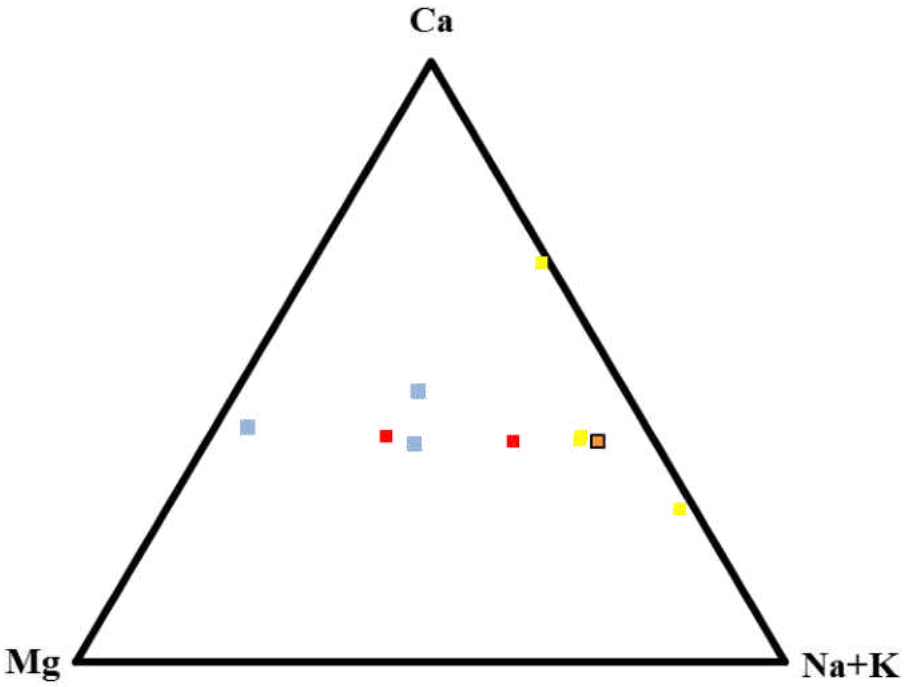

Figure 26- Ternary diagram of Ca^{2+}, Mg^{2+}, and $Na^{+}+K^{+}$ proportions for water samples. The concentrations were normalized to the sum of the concentrations. Light blue are miscellaneous acidic mud pots, red is the acidic red stream, orange is the near-neutral travertine spring, and yellow is the white stream. Proportions of Ca^{2+} are relatively constant across the geothermal field, while Mg^{2+} proportions increase as the water becomes more acidic. Proportions of Na^{+} and K^{+} increase as the water becomes more neutral.

, and HCO_3^{-}) show their relative proportions. More acidic waters had a higher proportion of Mg^{2+} than other waters, but the proportions of Ca^{2+} remained relatively constant (Figure 26), except for the upper part of the white stream, above the beginning of the white coating (IN1714). Na^{+} and K^{+} proportions are higher in more neutral waters. While the acidic water has higher

concentrations of SO_4^{2-}, the white stream has comparable to even higher proportions of SO_4^{2-} relative to the acidic waters (Figure 27). This is likely because the acidic waters have a higher bicarbonate concentration, which would increase the bicarbonate proportion and decrease the

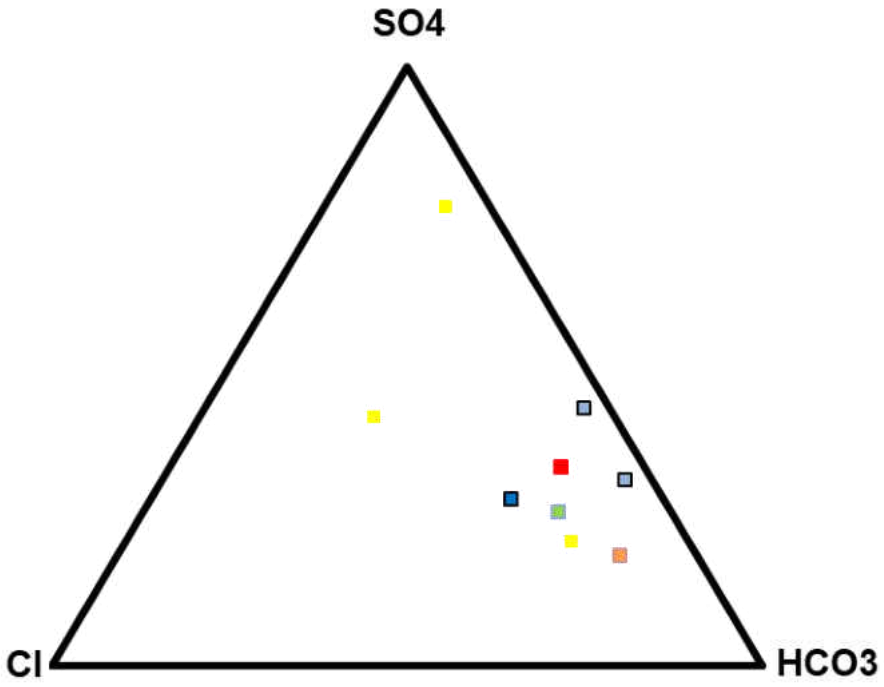

Figure 27- Ternary diagram of SO_4^{2-}, Cl^-, and HCO_3^- proportions for water samples. The concentrations were normalized to the sum of the concentrations. Light blue are miscellaneous mud pots, red is the red stream, orange is the travertine spring, green is confluence water, dark blue is a near-neutral hot spring, and yellow is the white stream. While in general the more acidic waters have higher concentrations of SO_4^{2-}, some samples from the more neutral white stream have concentrations comparable to the more acidic mud pots. The Cl^- proportions vary, but are all low, especially in the acidic water. The travertine spring has the highest proportion of bicarbonate, although many of the sites have similar proportions.

SO_4^{2-} proportion. The Cl^- proportions vary between sites but are low overall.

The increased acidity of these mud pots is likely due to acid-sulfate steam heating, and they are capable of mobilizing more cations out of the substrate than the more neutral sites. The travertine-depositing spring is the main exception to this, having 12.93 mg/L of K^+, 71.06 mg/L of Na^+, 12.09 mg/L of Mg^{2+} and 55.99 mg/L of Ca^{2+}. The large amount of Ca^{2+} present is precipitating out to form the extensive travertine precipitates that dominate the spring and surrounding area. Both the travertine spring and the sinter spring have high concentrations of Na^+, which is one of the indicators of an influx of NaCl hydrothermal water (Arnórsson et al., 1983; Kaasalainen and Stefánsson, 2011). Typically, both Na^+ and Cl^- would be indicators, but the waters for these sites have similar Cl^- concentrations to the rest of the geothermal field. NaCl hydrothermal water is formed when geothermal fluids experience decoupling and their volatiles

Sample	pH	K	Na	Mg	Ca	Fe2+	HCO3-	Cl-	SO4
IN1701	7.79	12.93	71.06	12.09	55.99	0.10	288.36	11.75	ND
NG-7	9.02	30.60	173.20	0.02	0.56	-	-	113.70	15.60
Reykjanes	6.38	1,720.00	11,150.00	1.44	1,705.00	0.33	-	22,835.00	28.40

Table 10- Major cations and anions present in the travertine spring (IN1701), a deep borehole in the Nesjavellir geothermal field (between 1000 to 1500 m) (NG-7), and a borehole in the Reykjanes Peninsula (Reykjanes). The hydrothermal water at depth in the Nesjavellir field is more alkaline than the surface water present at the travertine spring and has higher Na^+ and Cl^- concentrations than the surface waters. The water present in Nesjavellir has no seawater input. The geothermal field in Reykjanes does, and has resulted in drastically higher Na^+ and Cl^- concentrations due to the influx of seawater. NG-7 data from Mutonga et al. 2010, and Reykjanes data from Arnorsson et al. 1983.

rises to the surface with the steam produced. The remaining volatile-depleted fluid is the NaCl fluid, so named because of its high concentration of both elements. The source of these elements is leaching from the basalt, with some of the Cl^- being magmatic in origin (Arnórsson et al., 1983; Kaasalainen and Stefánsson, 2011). While Na^+ and Cl^- are concentrated relative to meteoric water, this does not indicate a seawater input. Borehole data from the Reykjanes peninsula show that a seawater-influenced hydrothermal fluid has Na^+ and Cl^- concentrations

over fifty times higher than geothermal fields further from the coast (Table 10). The water at both the travertine and sinter springs has high concentrations of Na^+ relative to other sites in this study, but do not indicate a pure NaCl hydrothermal water input. Rather, the water is more likely a mixture of NaCl waters and ground or meteoric water, or possibly a steam-depleted fluid (Kaasalainen and Stefánsson, 2012).

5.3 Overall water-rock interaction, mineral formation, and water chemistry at the surface

The hydrothermal features of the Nesjavellir and Hveragerdi geothermal fields exhibit a wide variety of environments that have resulted in different mineral assemblages and geochemical patterns throughout the fields. Several of the precipitate products at these hydrothermal features have formed due to the changing environments as the geothermal fluid ascends to the surface. A common feature of hot springs and mud pots of Nesjavellir is the presence of Fe-sulfides and/or native sulfur. For the more acidic environments, this is fairly common in the presence of high concentrations of S^{2-}. The oxidation of H_2S proceeds once exposed to atmospheric O_2, forming the abundant H_2SO_4 that dominates the chemistry of the acidic waters (Kaasalainen and Stefánsson, 2011). The presence and abundance of native sulfur and pyrite in these acidic, oxidizing conditions point to reducing conditions at a shallow depth. Once exposed to the oxidizing conditions, pyrite can oxidize and weather, releasing solutes that are incorporated into a variety of sulfates, including melanterite, halotrichite, magnesiocopiapite, pickeringite, aluminite ($Al_2SO_4(OH_4)\cdot 7H_2O$), and natrojarosite (King and McSween, 2005), all of which have been observed as a precipitate near or as a constituent of mud in the various hot springs and hydrothermal features of Nesjavellir. These conditions can also form rhomboclase, which often forms with pyrite.

The hydrothermal streams represent very different environments, which resulted in different coatings. The near-neutral white stream likely obtained its white elemental sulfur coating via oxidation of H_2S, somewhat similar to the more acidic waters. However, for more neutral waters, the oxidation of H_2S is a slower process, and follows the oxidation of S^{2-} into native sulfur, which then interacts with aqueous dissolved sulfur to form S_x^{2-}, a zero-valent sulfur species (Kaasalainen and Stefánsson, 2011). In this process, elemental sulfur readily precipitates out. The white stream's ubiquitous white sulfur coating likely formed in this manner. On the other side of the gully, the red stream's biofilm was created by the red stream's microbial community. The microbes present in the stream influence mineral precipitation and the stream's redox conditions, likely by oxidation of the stream's aqueous Fe^{2+} and S^{2-}. As the streams merge, the confluence waters are primarily influenced by white stream water, with ion concentrations, pH, and ORP being very similar to the white stream. However, pH is a little lower than the white stream, and several cation and anion concentrations (Mg^{2+}, Ca^{2+}, Fe^{2+}, and SO_4^{2-}) are higher than the white stream inputs, reflecting the red stream input.

While the red and white hydrothermal streams exhibit different environments, a seasonal trend is readily apparent in both streams, and in other hydrothermal sites as well. From the 2016 to the 2017 season, the red and white streams show an increase in concentration of K^+, Na^+, Mg^{2+}, and Ca^{2+} and a decrease in Cl^- and SO_4^{2-}. While the Cl^- concentrations are fairly similar across the geothermal fields, regardless of hydrothermal environment (11.84 mg/L for the acid mud pot near the red stream and 12.81 mg/L for the sinter spring in the Hveragerdi field) or year sampled (12.5 mg/L for red stream in 2016 and 11.68 mg/L in 2017) (Figure 16), higher SO_4^{2-} concentrations are associated with lower pH values and higher ORP. As the sulfate values decreased from 2016 levels to 2017 levels (96.56 mg/L to 33.11 mg/L), the pH of the red stream

increased and ORP decreased, suggesting that the SO_4^{2-} concentration is a major control on the acidity of the hydrothermal environment (Figure 28). This illustrates year to year, or potentially

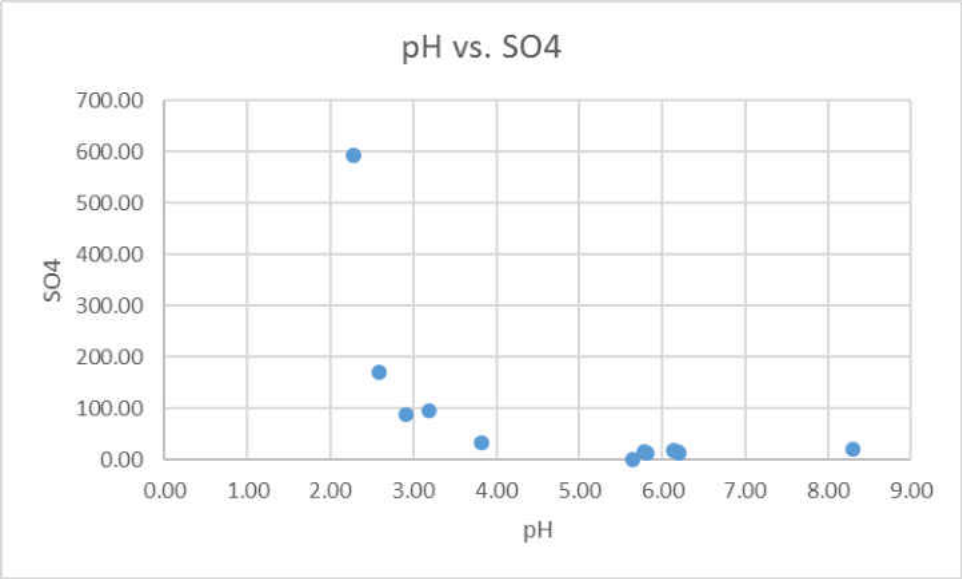

Figure 28- Plot of pH vs. SO_4^{2-}. SO_4^{2-} concentrations are in mg/L. As pH increases, SO_4^{2-} concentration decreases, suggesting that SO_4^{2-} concentrations influence pH.

seasonal, differences in ion concentrations and hydrothermal conditions.

5.4 Formation of hydrothermal waters and their impact

Formation of acid-sulfate hydrothermal environments such as the acidic hot springs and mud pots throughout Nesjavellir begins at depth, where the ascending geothermal aquifer waters are boiled due to depressurization (Kaasalainen and Stefánsson, 2012). Once boiling, the geothermal water experiences a phase segregation, where steam escapes from the aquifer fluid. This steam is rich in various volatiles, including H_2S and CO_2. The steam alters the host rock as it ascends, which can form reduced phases such as pyrite. Once it reaches oxygenated, cold groundwater or surface water, the H_2S in the steam will oxidize into H_2SO_4 due to the dissolved oxygen in groundwater or atmospheric O_2 (Kaasalainen and Stefánsson, 2012). Due to the low pH of the steam, this is a relatively quick process that forms a strongly oxidizing environment

(Kaasalainen and Stefánsson, 2011). A byproduct of the oxidation of H_2S is abundant elemental sulfur forming in the spring. Pyrite is likely present because the oxidizing conditions are limited to the surface, or because of a relatively recent change in the hydrothermal environment (Figure 29). The acidic and oxidizing environment eventually dissolves the pyrite, forming large concentrations of SO_4^{2-} which precipitate out as Al-, Ca-, Mg-, and Fe-sulfates (Arnórsson et al., 1983; King and McSween, 2005). The surrounding rock and soil are then extensively leached of

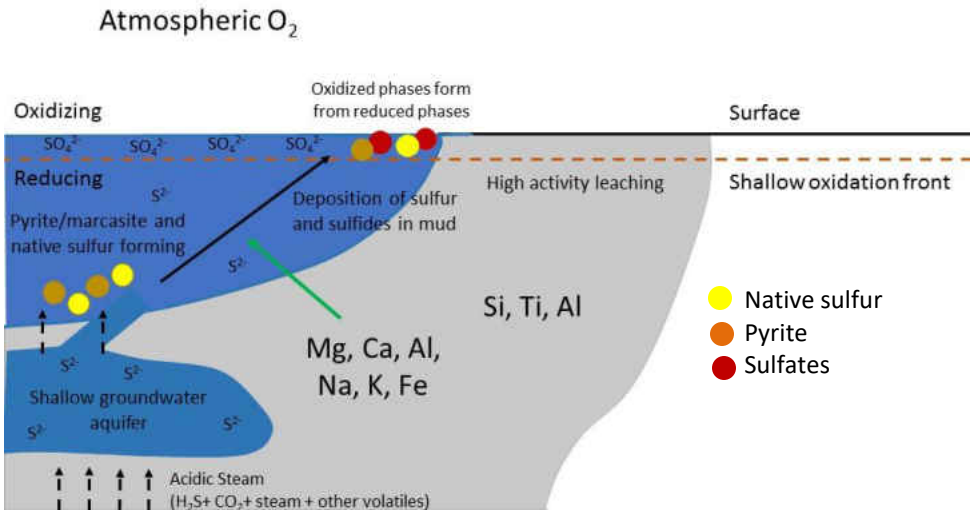

Figure 29- Conceptual model for leaching and mineral formation in acid-sulfate mud pots. Acidic steam heats a shallow aquifer, acidifying it and producing reducing conditions. Near-surface environments will be more oxidizing. Leaching of mobile cations will occur, residually enriching Si, Ti, and occasionally Al.

more mobile cations, leaving various clays and residual minerals such as amorphous silica and anatase.

Neutral to alkaline hydrothermal environments like the travertine spring and Hveragerdi's sinter spring likely had a similar origin to the acid-sulfate features. The geothermal fluid that underwent depressurization boiling to produce the steam/vapor phase continued to ascend and mixed with shallow ground and surface water to reach the surface to form NaCl hydrothermal

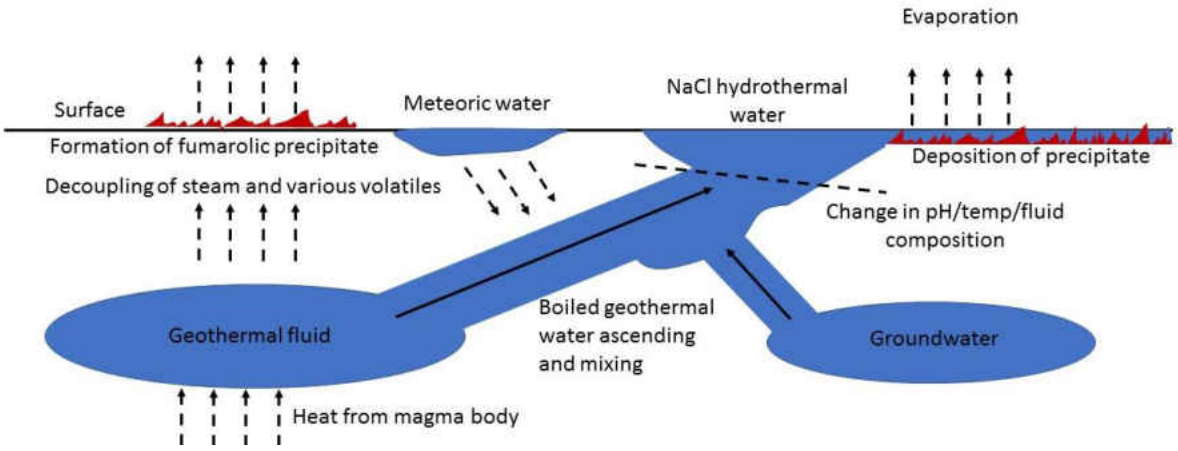

Figure 30- Conceptual model for hydrothermal processes in neutral to alkaline hot springs, depicting boiling of the fluid, mixing with other waters while ascending, and precipitating travertine or sinter. The precipitation is tied to changes in pH, temperature, mixing of fluids, and evaporation of fluid.

waters (Kaasalainen and Stefánsson, 2012). The water that reaches the surface will have elevated Na^+ concentrations, which can be seen in both the travertine spring and the sinter spring. However, the waters produced at these sites have around the same concentration of Cl^- as other, more acidic areas, while the Cl^- concentrations should be higher. This discrepancy may be because the waters are not purely NaCl waters, but perhaps a mixture of a variety of waters dominated by geothermal fluids (Figure 30). As the hydrothermal waters reach the surface, one or several factors (potentially including temperature changes, solution mixing, evaporation, or changes in pH) induces precipitation of a mineral phase, based on the aqueous phases in the water. The Hveragerdi sinter spring precipitates silica, and from the presence of layered deposits, this spring has been depositing silica for a long time. The travertine spring has extensive fossil deposits that also show a stable environment for precipitating travertine over an extended time. These environments are promising areas for microbial communities to flourish, as is evidenced by the microbial structures preserved in the canal walls of the travertine spring.

Near-neutral environments are widespread throughout Nesjavellir, and likely represent mixtures of NaCl water, acid-sulfate waters, and ground/surface water. The northern spring exhibits leaching of the surrounding soil, but the presence of minimally-altered plagioclase in the soil at depth indicates a more moderate environment than at the acid-sulfate sites. Abundant sulfates in the form of halotrichite and natrojarosite point to processes related to the oxidation of pyrite in this environment (Figure 31).

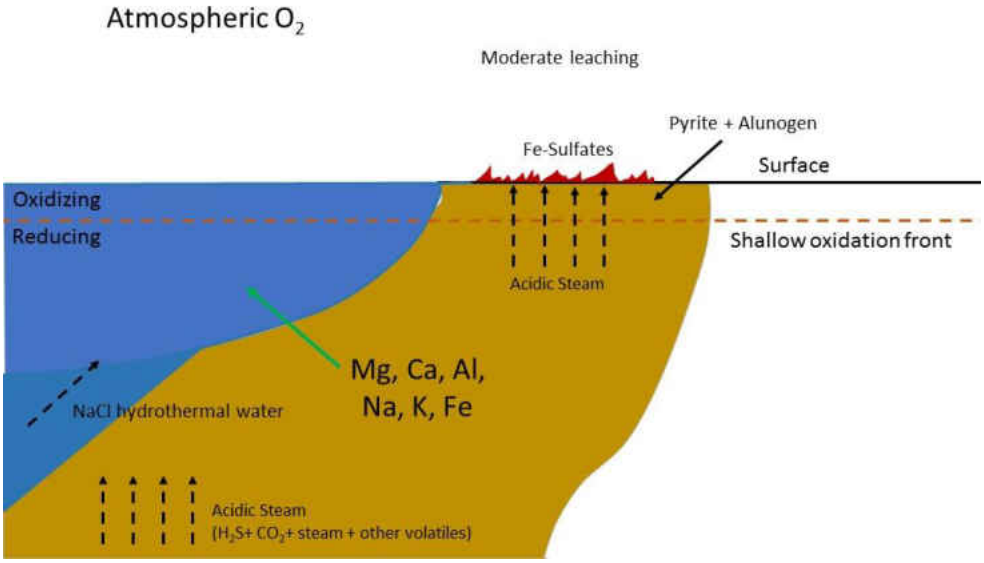

Figure 31- Conceptual model for hydrothermal processes in near-neutral hot springs, depicting mixing of boiled NaCl hydrothermal water and acidic steam, producing a moderately leaching environment. Remnant plagioclase is still present in the soil, and both pyrite and alunogen are present in shallow soil.

The hydrothermal streams are sourced from various hydrothermal features throughout the gully in which they are found, the red stream more so than the white stream. The red stream sources its water from further uphill than the white stream, where the red stream interacts with various mud pots and springs too dangerous to sample. These features likely influence the red stream, contributing water, lowering its pH, and increasing the ORP. Downstream, the water cools and microbial communities influence the redox of the waters, oxidizing the reduced Fe and

S for sustenance. The Fe then precipitates out as nanophase Fe-oxides. The white stream is likely a mixture of a steam phase and shallow ground water, which is flowing downhill towards the red stream. Due to the near-neutral pH of the white stream, the oxidation of H_2S is slower than in more acidic environments, and oxidizes into elemental sulfur before then oxidizing into sulfate. The precipitation of native sulfur is a common by-product of this process, and is precipitated out as the water flows downstream, creating the white coating characteristic of the stream (Figure 32).

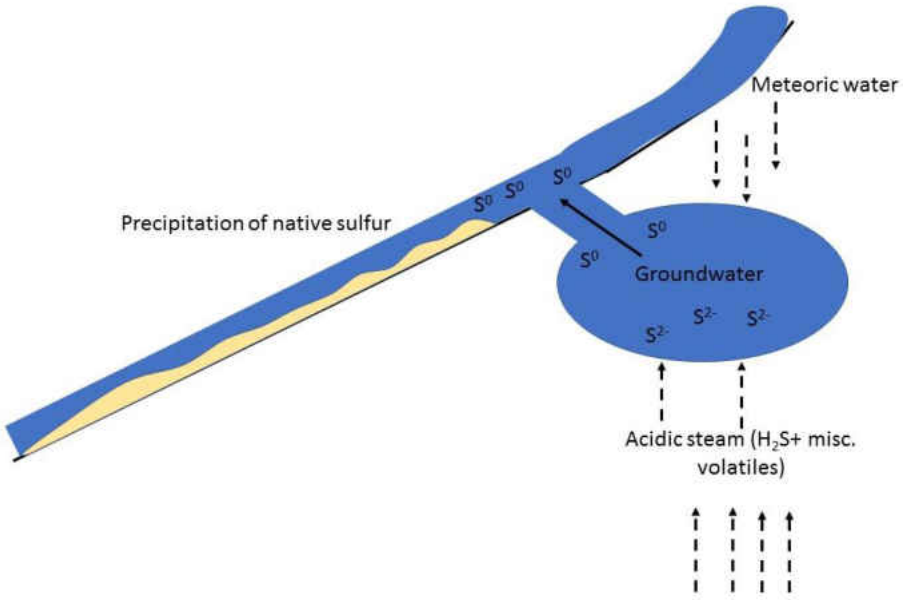

Figure 32- Conceptual model for formation and deposition of the white sulfur coating in the white stream. The precipitation is tied to the slow oxidation of sulfur in near-neutral pH waters, which involves deposition of native sulfur.

6. Implications for Mars

Comparing mineral deposits and chemical trends of the Nesjavellir and Hveragerdi geothermal fields to Martian analogues in Gusev crater requires consideration of several key differences between these two environments. Icelandic surface hydrothermal environments are

Sample	IN1616	Adirondack	Bounce Rock	Shergotty	Jake_Matijavic (1)
SiO_2	47.45%	45.30%	50.81%	51.30%	52.54%
TiO_2	2.20%	0.49%	0.78%	0.49%	0.52%
Al_2O_3	14.76%	10.42%	10.10%	6.88%	16.73%
Fe_2O_3	13.15%	21.09%	15.60%	19.40%	9.79%
MnO	0.20%	0.42%	0.43%	0.40%	0.15%
MgO	6.48%	11.90%	6.40%	9.30%	3.76%
CaO	12.20%	7.76%	12.50%	9.60%	7.35%
Na_2O	1.97%	2.09%	1.30%	1.39%	7.35%
K_2O	0.19%	0.03%	0.10%	0.17%	2.30%
P_2O_5	0.25%	0.54%	-	0.67%	0.52%
LOI	-0.49%	-	-	-	-
Sum	98.99%	99.81%	-	-	-

Table 11- Composition of basalt substrates in Iceland and in various localities on Mars, in weight percentages. '-' is not determined. Adirondack concentrations obtained from McSween et al. (2006), Bounce Rock concentrations from Rieder et al. (2004), Shergotty concentrations from Lodders (1998), and Jake_Matijavic concentrations from Schmidt et al. (2014).

open hydrothermal systems with abundant O_2 in a very wet environment. Many of the cations that are leached by these systems (Mg^{2+}, Ca^{2+}, Na^{+}, and others) and more soluble sulfates are mobilized out of the hydrothermal system. Martian conditions at present are significantly different. Current terrestrial conditions include abundant O_2 in a thick atmosphere which supports warm and wet environments, while the present O_2 concentration on Mars is low (~0.13%) and its atmosphere is much thinner (Dehouck et al., 2016). Mars' thin atmosphere and its distance from the sun has led Mars to be a cold and dry planet that cannot sustain stable surface aqueous environments (Cabrol et al., 2006). The environment of Mars may have been more similar to terrestrial conditions in the past, but specific characteristics, such as atmospheric composition and abundance of water, are not yet well constrained. The presence of Fe-sulfates (likely formed by the weathering of Fe-sulfides) does indicate that oxidizing and acidic conditions may have occurred at least locally (Dehouck et al., 2012).

Another significant difference between the two areas is the composition of the protolith basalt. Table 11 provides compositions for various Martian basalts, including the Gusev crater floor flood basalt (Adirondack), float rock in both Meridiani Planum and Gale crater (Bounce Rock and Jake Matijavik), and meteorites (Shergotty). The tholeiitic basalts of Iceland differ in several elements compared to Martian samples, with higher TiO_2 and Al_2O_3 in Icelandic basalt (2.20 wt% and 14.76 wt% respectively) than in Martian material (<0.70 wt% and <10.50 wt% respectively). However, iron occurs in higher concentrations in the Martian samples, with concentrations of 15.60 wt% Fe_2O_3T (Bounce Rock), 19.40 wt% (the Shergotty meteorite), and 21.09 wt% (Adirondack)(Table 10) (Lodders, 1998; Rieder et al., 2004; McSween et al., 2006). The exception to this trend is the Jake_Matijavic float rock from Gale Crater, which has a lower Fe_2O_3 concentration than IN1616 (9.79 wt% vs. 13.15 wt%) and higher Al_2O_3 and SiO_2 concentrations (16.73 wt% and 52.54 wt%) than the Icelandic basalt (Schmidt et al., 2014). The CaO concentrations of Bounce Rock and the Icelandic basalt are very similar, with Bounce Rock at 12.50 wt% and the Icelandic basalt at 12.20 wt%, with other Martian samples having between 7-10 wt%. MgO is lowest in the Gale Crater sample with 3.76 wt%, with low concentrations in Bounce Rock and Icelandic basalt (6.40 wt% and 6.48 wt%, respectively), and the highest concentrations in the Shergotty meteorite (9.3 wt% MgO) and Adirondack (11.9 wt%). These differences have a crucial influence over the available elements entering these hydrothermal environments, which determines what minerals are formed. For instance, Al-sulfates are common throughout Nesjavellir, but are much less common on Mars.

6.1 Paso Robles soils class

The Paso Robles soil class consists of yellowish-whitish soil that contains likely alteration products. These localities represent some of the more altered areas of the Columbia

Hills. Paso Robles soils have high SO_3 concentrations (29.6 wt%), consistent with the abundant sulfate minerals observed in these deposits (Ming et al., 2008). Mg-, Ca-, and Fe- sulfates are found in these soils, with ferric (Fe^{3+}) sulfates being the most abundant. Also found in these deposits are Ca- and Fe-phosphates, hematite, amorphous silica, and other minor phases. There are several possibilities for what the ferric sulfates could be, including ferricopiapite, jarosite, and rhomboclase, among others. The Paso Robles soils can be found in the Paso Robles, Arad (Dead Sea), and Tyrone/Eastern Valley areas. The Paso Robles locality is on a slope, while the Arad and Tyrone localities are in geomorphic lows (Wang et al., 2008; Yen et al., 2008).

Deposits formed in the Nesjavellir geothermal field are mineralogically similar to the Paso Robles soil class. Abundant Fe-sulfates are present in several acidic mud pots and a near-neutral hot spring in Nesjavellir. These Fe-sulfates include halotrichite, rhomboclase, melanterite, and natrojarosite. The Mg-sulfates pickeringite and magnesiocopiapite are precipitating on the surface in an area with elevated temperature, likely reflecting diffuse fumarolic conditions. Many of the sulfates listed form from the oxidation and weathering of an Fe-sulfide, usually pyrite (King and McSween, 2005). One of the oxidation products listed, melanterite, will alter further in increasingly acidic environments into jarosite. The presence of rhomboclase and a variety of Fe-sulfates often associated with the oxidation of sulfides on Mars indicates that the hydrothermal environment which formed the Paso Robles soils class could have been reducing at depth and oxidizing at the surface. This may have been due to atmospheric contact with the steam-heated sites, which likely oxidized the H_2S influx and produced the SO_4^{2-} which acidified the hydrothermal sites (Wang et al., 2008; Yen et al., 2008; Kaasalainen and Stefánsson, 2011). However, the presence of several ferric sulfates around a near-neutral spring (IN1601) in the Nesjavellir geothermal field (halotrichite and natrojarosite) shows that a

dominantly acidic environment is not necessary for the formation of these minerals. Some of the Nesjavellir sites are located in topographic lows, such as the northern spring and the southern mud pot, while several are located at the base of slopes, such as the hot spring associated with the red stream. Several of these sites exhibit heterogeneous distribution of sulfates similar to Arad, while several other sites show a more homogenous distribution similar to Tyrone.

During the initial analysis of the Paso Robles soil class, the deposits were inferred to have formed under acid-sulfate fumarolic conditions (Squyres et al., 2008; Yen et al., 2008). The type locality for the Paso Robles soils suggests that this is the case, with the soils appearing to be spatially discontinuous and of heterogeneous distribution. While the Arad site is more spatially continuous than Paso Robles, the soils there appear to have a heterogeneous distribution as well (Wang et al., 2008). The heterogeneous distributions present in both of these sites suggest a more fumarolic environment with point sources of acidic, sulfuric gases. However, Tyrone is both spatially continuous and has a homogenous distribution, consistent with a more aqueous environment. A more aqueous environment for Tyrone, but also Arad and Paso Robles, is evidenced by the excess amount of Fe_2O_3 + FeO present in the soils, which implies that there was enough fluid to transport the Fe^{3+} to the site of deposition (Hausrath et al., 2013).

The sites studied in Iceland are all aqueous hot springs, mud pots, and streams, with a few areas altered by acid-sulfate steam. Several of the sites show some heterogeneous distribution with their precipitates, as with the northern spring. These sites have areas rich in sulfates while other areas are residually enriched with clays, anatase, and silica. The distributions observed at the Icelandic sites are similar to ones found at Paso Robles and Arad in the Columbia Hills on Mars, indicating that a more aqueous environment is possible for at least Arad. If Paso Robles were more aqueous, the area of the soils would be expected to be larger and extend

further downslope. Given Arad's larger area and location on a geomorphic low, a more aqueous environment is possible (Wang et al., 2008).

6.2 Preservation of biological activity and habitability

Digitate silica-rich opal-A nodules had been found east of Home Plate in the locality Eastern Valley and in the Tyrone site, and due to the abundant sulfates in the Tyrone site, as well as high TiO_2 present in the nodules relative to other soils, the nodules present at Tyrone were attributed to acid-sulfate leaching at a high enough water:rock ratio to allow the formation of the nodules (Squyres et al., 2008). Due to their similar morphology, the Eastern Valley nodules were initially attributed to the same process. However, later work by Ruff and Farmer (2016) shows that the nodules present in Eastern Valley could be the product of biological activity under near-neutral conditions, and makes a strong case with a side-by-side comparison of the Martian nodules and digitate silica nodules found in the El Tatio geothermal field in Chile. Silica nodules in terrestrial geothermal fields form when silica in alkali-chloride hydrothermal fluids polymerizes and precipitates out as opal-A. The opal-A can nucleate on a variety of surfaces, including on microorganisms (Konhauser et al., 2004). The deposited silica sinter then undergoes a series of mineralogic, morphologic, and crystallographic changes due to diagenesis. As time since precipitation increases under terrestrial conditions, the opal-A morphs into a variety of opal phases before finally reaching stability as microcrystalline quartz (Lynne et al., 2007). Any evidence of microbial activity is typically destroyed in this process. However, the Martian silica nodules are still composed of opal-A, which indicates that these nodules may still hold evidence of biological activity, if there was activity present. Further work presented in Ruff et al. (2011) shows that while the nodules at Tyrone were likely the products of acid-sulfate leaching, consistent with Squyres et al., 2008, the nodules studied in Eastern Valley were not. The Eastern

Valley nodules were not found with sulfur-containing minerals, suggesting an origin under neutral conditions.

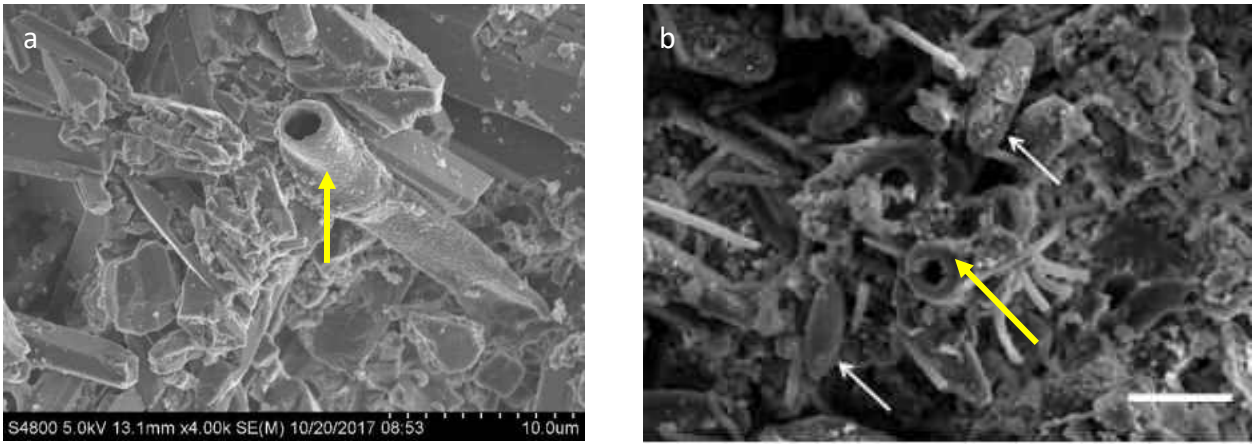

Figure 33- A comparison between work done in this study (a) and work done in Ruff and Farmer (2016) (b). The tube structures (indicated by the yellow arrows) are similar in morphology. White arrows in (b) The white bar represents 20 microns.

The neutral travertine spring in Nesjavellir shows somewhat similar morphological structures to the sites in Eastern Valley and El Tatio, and the siliceous microstructures are similar to structures observed in El Tatio sinter (Figure 33). However, the travertine spring is not comparable to these sites, however the Nesjavellir travertine deposit is dominated by carbonate rather than silica sinter. The combination of high water:rock ratios relative to both Mars and El Tatio and its travertine composition makes it an unsuitable analogue. The silica sinter observed at the Hveragerdi field consisted of thin, layered deposits, morphologically different from the digitate sinter nodules observed at El Tatio or the nodules of the Eastern Valley on Mars. SEM analyses were not attempted on Hveragerdi sinter, so any microbiological similarity with the El Tatio sinter cannot be determined at present. Mineralogically, the two sites both contain primarily amorphous silica, although El Tatio also has trace amounts of gypsum, cahnite ($Ca_4B_2As_2O_{12}\cdot 4H_2O$), and other As-bearing phases (Nicolau et al., 2014) while Hveragerdi has some calcite and halite in the precipitate and some clay in the layered deposits. The SiO_2 and

TiO_2 concentrations for Hveragerdi (>85 wt% and <0.40 wt%, respectively) are typical for a precipitated sinter, and while there is little data on the major elements of El Tatio, the Columbia Hills' silica-rich rock class Elizabeth Mahon has SiO_2 and TiO_2 concentrations of 71.8 wt% and 0.67 wt%, respectively, while the Gertrude Weiss soils are 90.3 wt% and 1.21 wt%, respectively (Ming et al., 2008). Both classes have higher TiO_2 concentrations than the Adirondack substrate (0.49 wt%). Furthermore, the water forming the nodules in El Tatio is less than 40°C and pH 6.5-7.5 (Ruff and Farmer, 2016). The waters for both the travertine and sinter spring are above 60°C (67°C and 99.3°C, respectively), and the sinter spring is more alkaline (pH 8.30) than El Tatio.

Despite not being directly comparable to El Tatio in Chile or Eastern Valley in the Columbia Hills of Mars, the neutral-alkaline environments studied here host life, and at least in the travertine spring, preserve it. For some microbial communities, a neutral environment is not necessary for survival, as can be seen with the red stream. The microbial communities present are thriving in an acidic, oxidizing environment, likely forming nanophase Fe-oxides as a byproduct of their oxidation of S and Fe. It is uncertain if the red biofilm is capable of preserving microbial activity or even maintaining its structure outside of an aqueous environment. Further study could possibly lead to another signature of productive lifeforms on Mars.

7. Conclusions

This study investigated hydrothermal alteration of Mars-like basalt and precipitation in acid-sulfate, near-neutral, and neutral-alkaline environments. The processes forming the mineralogical and geochemical trends in the Nesjavellir geothermal field and the sinter spring of the Hveragerdi geothermal field were investigated, providing context and insight into the formation of various soils and outcrops in the Columbia Hills of Mars. This study concludes that:

1. The compositions of alteration products in acidic environments are influenced by the leaching and mobilization of most major elements (Fe_2O_3, MgO, CaO, Na_2O, and K_2O).
2. Ubiquitous pyrite in acidic and near-neutral sites, coupled with sulfate minerals in surface precipitates, points to reducing conditions at depth that become oxidizing at or just below the surface waters.
3. SO_4^{2-} concentrations co-vary with pH and the ORP, and may be a control on the acidity of hydrothermal environments in the Nesjavellir geothermal field.
4. Weathering and oxidation of pyrite allowed the formation of the SO_4^{2-} used by the Fe- and Mg-sulfates observed in both acidic and near-neutral sites, with Fe-bearing sulfates as the most abundant. These sites resemble the Paso Robles-type soil deposits at Arad and Paso Robles on Mars, which could have formed in similar environments.
5. The travertine in the travertine spring likely formed from a temperature or pH change coupled with an evaporation of the water. The spring hosts an active microbial community, as evidenced by the biological microstructures silicified in the travertine walls.
6. The almost pure native sulfur white coating in the white stream likely formed from the oxidation of H_2S, which is a relatively slow reaction.
7. While the alkaline hot spring of the Hveragerdi geothermal field is actively precipitating silica sinter, the resulting sinter occurs as thin coatings, morphologically different from the opal-A nodules of the Columbia Hills on Mars.

8. References

Abramov, O., Kring, D.A., 2005. Impact-induced hydrothermal activity on early Mars. J. Geophys. Res. E Planets 110, 1–19. doi:10.1029/2005JE002453

Achenbach, L., Bailey, J., Barnes, R., Baross, J., Bertka, C., Boston, P., Boyd, E., Cable, M.,

Chen, I., Ciesla, F., Des Marais, D., Domagal-Goldman, S., Cook, J.E., Goldman, A., Hud, N., Laine, P., Lloyd, K., Lyons, T., Meadows, V., Mix, L., Mojzsis, S., Muller, U., Pasek, M., Powell, M., Robinson, T., Rosenzweig, F., Schmidt, B., Seelig, B., Springsteen, G., Vance, S., Welander, P., Williams, L., Wordsworth, R., 2015. NASA Astrobiology Strategy 2015, NASA Astrobiology. doi:10.1017/CBO9781107415324.004

Arnason, B., Theodorsson, P., Björnsson, S., Saemundsson, K., 1969. Hengill, a high temperature thermal area in Iceland. Bull. Volcanol. 33, 245–259. doi:10.1007/BF02596720

Arnórsson, S., Gunnlaugsson, E., Svavarsson, H., 1983. The chemistry of geothermal waters in Iceland. II. Mineral equilibria and independent variables controlling water compositions. Geochim. Cosmochim. Acta 47, 547–566. doi:10.1016/0016-7037(83)90277-6

Arvidson, R.E., Ruff, S.W., Morris, R. V., Ming, D.W., Crumpler, L.S., Yen, A.S., Squyres, S.W., Sullivan, R.J., Bell, J.F., Cabrol, N.A., Clark, B.C., Farrand, W.H., Gellert, R., Greenberger, R., Grant, J.A., Guinness, E.A., Herkenhoff, K.E., Hurowitz, J.A., Johnson, J.R., Klingelhöfer, G., Lewis, K.W., Li, R., McCoy, T.J., Moersch, J., McSween, H.Y., Murchie, S.L., Schmidt, M., Schröder, C., Wang, A., Wiseman, S., Madsen, M.B., Goetz, W., McLennan, S.M., 2008. Spirit Mars Rover Mission to the Columbia Hills, Gusev Crater: Mission overview and selected results from the Cumberland Ridge to Home Plate. J. Geophys. Res. E Planets 113. doi:10.1029/2008JE003183

Barlow, N.G., 2010. What we know about Mars from its impact craters. Bull. Geol. Soc. Am. 122, 644–657. doi:10.1130/B30182.1

Bibring, J.-P., Langevin, Y., Mustard, J.F., Poulet, F., Arvidson, R., Gendrin, A., Gondet, B., Mangold, N., Pinet, P., Forget, F., Omega team, 2006. Global Mineralogical and Aqueous Mars History Derived from OMEGA/Mars Express Data. Science (80-.). 312, 400–404.

Bishop, J.L., Dobrea, E.Z.N., Mckeown, N.K., Parente, M., Ehlmann, B.L., Michalski, J.R., Milliken, R.E., Poulet, F., Swayze, G.A., Mustard, J.F., Murchie, S.L., Bibring, J.-P., 2008. Phyllosilicate Diversity and Past Aqueous Activity Revealed at Mawrth Vallis, Mars. Source Sci. New Ser. 321, 830–833. doi:10.1126/science.1159699

Bishop, J.L., Loizeau, D., McKeown, N.K., Saper, L., Dyar, M.D., Des Marais, D.J., Parente, M., Murchie, S.L., 2013. What the ancient phyllosilicates at Mawrth Vallis can tell us about possible habitability on early Mars. Planet. Space Sci. 86, 130–149. doi:10.1016/j.pss.2013.05.006

Bishop, J.L., Schiffman, P., Murad, E., Dyar, M.D., Drief, A., Lane, M.D., 2007. Characterization of alteration products in tephra from Haleakala, Maui: A visible-infrared spectroscopy, Mössbauer spectroscopy, XRD, EMPA and TEM study. Clays Clay Miner. 55, 1–17. doi:10.1346/CCMN.2007.0550101

Black, S.R., Hynek, B.M., 2017. Characterization of terrestrial hydrothermal alteration products with Mars analog instrumentation: Implications for current and future rover investigations. Icarus submitted, 1–25. doi:10.1016/j.icarus.2017.10.032

Bourgeois O, Dauteuil O, Van Vliet-Lanoe B (1998) Pleistocene subglacial volcanism in

Iceland: tectonic implications. EPSL 164: 165-178.

Browne, P.R.L., 1978. Hydrothermal alteration in active geothermal fields. Annu. Rev. Earth Planet. Sci. 6, 229–250.

Byers, H.L., McHenry, L.J., Grundl, T.J., 2016. Forty-Nine Major and Trace Element Concentrations Measured in Soil Reference Materials NIST SRM 2586, 2587, 2709a, 2710a and 2711a Using ICP-MS and Wavelength Dispersive-XRF. Geostand. Geoanalytical Res. 40, 433–445. doi:10.1111/j.1751-908X.2016.00376.x

Cabrol, N.A., Farmer, J.D., Grin, E.A., Ritcher, L., Soderblom, L., Li, R., Herkenhoff, K., Landis, G.A., Arvidson, R.E., 2006. Aqueous processes at Gusev crater inferred from physical properties of rocks and soils along the Spirit traverse. J. Geophys. Res. E Planets 111, 1–15. doi:10.1029/2005JE002490

Cousins, C.R., Crawford, I.A., Carrivick, J.L., Gunn, M., Harris, J., Kee, T.P., Karlsson, M., Carmody, L., Cockell, C., Herschy, B., Joy, K.H., 2013. Glaciovolcanic hydrothermal environments in Iceland and implications for their detection on Mars. J. Volcanol. Geotherm. Res. 256, 61–77. doi:10.1016/j.jvolgeores.2013.02.009

Davis, J.M., Balme, M., Grindrod, P.M., Williams, R.M.E., Gupta, S., 2016. Extensive Noachian fluvial systems in Arabia Terra: Implications for early Martian climate. Geology 44, 847–850. doi:10.1130/G38247.1

Dehouck, E., Chevrier, V., Gaudin, A., Mangold, N., Mathé, P.E., Rochette, P., 2012. Evaluating the role of sulfide-weathering in the formation of sulfates or carbonates on Mars. Geochim. Cosmochim. Acta 90, 47–63. doi:10.1016/j.gca.2012.04.057

Dehouck, E., Gaudin, A., Chevrier, V., Mangold, N., 2016. Mineralogical record of the redox conditions on early Mars. Icarus 271, 67–75. doi:10.1016/j.icarus.2016.01.030

Des Marais, D.J., Nuth, J.A., Allamandola, L.J., Boss, A.P., Farmer, J.D., Hoehler, T.M., Jakosky, B.M., Meadows, V.S., Pohorille, A., Runnegar, B., Spormann, A.M., 2008. The NASA Astrobiology Roadmap. Astrobiology 8, 715–730. doi:10.1089/ast.2008.0819

Filiberto, J., Schwenzer, S.P., 2013. Alteration mineralogy of Home Plate and Columbia Hills-Formation conditions in context to impact, volcanism, and fluvial activity. Meteorit. Planet. Sci. 48, 1937–1957. doi:10.1111/maps.12207

Foulger, G.R., Toomey, D.R., 1989. Structure and evolution of the Hengill-Grensdalur Volcanic Complex, Iceland: Geology, geophysics, and seismic tomography. J. Geophys. Res. 94, 17511. doi:10.1029/JB094iB12p17511

Franzson, H., Kristjánsson, B.R., Gunnarsson, G., Björnsson, G., Hjartarson, A., Steingrímsson, B., Gunnlaugsson, E., Gíslason, G., 2005. The Hengill-Hellisheiði Geothermal Field. Development of a Conceptual Geothermal Model. World Geotherm. Congr. 2005 24–29.

Geptner, A.R., Ivanovskaya, T.A., Pokrovskaya, E. V., 2005. Hydrothermal fossilization of microorganisms at the Earth's Surface in Iceland. Lithol. Miner. Resour. 40, 505–520. doi:10.1007/s10987-005-0048-2

Ghatan, G.J., Head, J.W., 2002. Candidate subglacial volcanoes in the south polar region of Mars: Morphology, morphometry, and eruption conditions. J. Geophys. Res. 107. doi:10.1029/2001JE001519

Golden, D.C., Ming, D.W., Morris, R. V., Mertzman, S.A., 2005. Laboratory-simulated acid-sulfate weathering of basaltic materials: Implications for formation of sulfates at Meridiani Planum and Gusev crater, Mars. J. Geophys. Res. E Planets 110, 1–15. doi:10.1029/2005JE002451

Grotzinger, J., 2009. Beyond water on Mars. Nat. Geosci. 2, 231–233. doi:10.1038/ngeo480

Hardardottir, V., 1983. The petrology of the Hengill volcanic system, southern Iceland. McGill University.

Hausrath, E.M., Golden, D.C., Morris, R. V., Agresti, D.G., Ming, D.W., 2013. Acid sulfate alteration of fluorapatite, basaltic glass and olivine by hydrothermal vapors and fluids: Implications for fumarolic activity and secondary phosphate phases in sulfate-rich Paso Robles soil at Gusev Crater, Mars. J. Geophys. Res. E Planets 118, 1–13. doi:10.1029/2012JE004246

Hynek, B., 2016. The great climate paradox of ancient Mars. Geology 44, 879–880. doi:10.1130/focus102016.1

Hynek, B.M., McCollom, T.M., Marcucci, E.C., Brugman, K., Rogers, K.L., 2013. Assessment of environmental controls on acid-sulfate alteration at active volcanoes in Nicaragua: Applications to relic hydrothermal systems on Mars. J. Geophys. Res. E Planets 118, 2083–2104. doi:10.1002/jgre.20140

Hynek, B.M., McCollom, T.M., and Rogers, K.L., 2011, Cerro Negro volcano, Nicaragua: An assessment of geological and potential biological systems on early Mars, *in* Garry, W.B., and Bleacher, J.E., eds., Analogs for planetary Exploration: Geological Society of America Special Paper 483, p. 279-285, doi: 10.1130/2011.2483(18).

Inskeep, W.P., Macur, R.E., Harrison, G., Bostick, B.C., Fendorf, S., 2004. Biomineralization of As(V)-hydrous ferric oxyhydroxide in microbial mats of an acid-sulfate-chloride geothermal spring, Yellowstone National Park. Geochim. Cosmochim. Acta 68, 3141–3155. doi:10.1016/J.GCA.2003.09.020

Jousset, P., Haberland, C., Bauer, K., Arnason, K., 2011. Hengill geothermal volcanic complex (Iceland) characterized by integrated geophysical observations. Geothermics 40, 1–24. doi:10.1016/j.geothermics.2010.12.008

Kaasalainen, H., Stefánsson, A., 2012. The chemistry of trace elements in surface geothermal waters and steam, Iceland. Chem. Geol. 330–331, 60–85. doi:10.1016/j.chemgeo.2012.08.019

Kaasalainen, H., Stefánsson, A., 2011. Sulfur speciation in natural hydrothermal waters, Iceland. Geochim. Cosmochim. Acta 75, 2777–2791. doi:10.1016/j.gca.2011.02.036

King, P.L., McSween, J.Y., 2005. Effects of H2O, pH, and oxidation state on the stability of Fe

minerals on Mars. J. Geophys. Res. E Planets 110, 1–15. doi:10.1029/2005JE002482

Konhauser, K.O., Ferris, F.G., 1996. Diversity of iron and silica precipitation by microbial mats in hydrothermal waters, Iceland: Implications for Precambrian iron formations. Geology 24, 323–326. doi:10.1130/0091-7613(1996)024<0323:DOIASP>2.3.CO

Konhauser, K.O., Jones, B., Phoenix, V.R., Ferris, G., Renaut, R.W., 2004. The Microbial Role in Hot Spring Silicification. Ambio 33, 552–558. doi:10.1579/0044-7447-33.8.552

Konhauser, K.O., Phoenix, V.R., Bottrell, S.H., Adams, D.G., Head, I.M., 2001. Microbial-silica interactions in Icelandic hot spring sinter: Possible analogues for some Precambrian siliceous stromatolites. Sedimentology 48, 415–433. doi:10.1046/j.1365-3091.2001.00372.x

Lodders, K., 1998. A survey of shergottite, nakhlite and chassigny meteorites whole-rock compositions.

Lynne, B.Y., Campbell, K.A., James, B.J., Browne, P.R.J., Moore, J., 2007. Tracking crystallinity in siliceous hot-spring deposits. Am. J. Sci. 307, 612–641. doi:10.2475/03.2007.03

Maclennan, J., Jull, M., McKenzie, D., Slater, L., Grönvold, K., 2002. The link between volcanism and deglaciation in Iceland. Geochemistry, Geophys. Geosystems 3, 1–25. doi:10.1029/2001GC000282

Manga, M., Patel, A., Dufek, J., Kite, E.S., 2012. Wet surface and dense atmosphere on early Mars suggested by the bomb sag at Home Plate, Mars. Geophys. Res. Lett. 39, 2–6. doi:10.1029/2011GL050192

Markússon, S.H., Stefánsson, A., 2011. Geothermal surface alteration of basalts, Krysuvik Iceland-Alteration mineralogy, water chemistry and the effects of acid supply on the alteration process. J. Volcanol. Geotherm. Res. 206, 46–59. doi:10.1016/j.jvolgeores.2011.05.007

Marzo, G.A., Davila, A.F., Tornabene, L.L., Dohm, J.M., Fairén, A.G., Gross, C., Kneissl, T., Bishop, J.L., Roush, T.L., McKay, C.P., 2010. Evidence for Hesperian impact-induced hydrothermalism on Mars. Icarus 208, 667–683. doi:10.1016/j.icarus.2010.03.013

McCollom, T.M., Robbins, M., Moskowitz, B., Berquõ, T.S., Jöns, N., Hynek, B.M., 2013. Experimental study of acid-sulfate alteration of basalt and implications for sulfate deposits on Mars. J. Geophys. Res. E Planets 118, 577–614. doi:10.1002/jgre.20044

McCoy, T.J., Sims, M., Schmidt, M.E., Edwards, L., Tornabene, L.L., Crumpler, L.S., Cohen, B.A., Soderblom, L.A., Blaney, D.L., Squyres, S.W., Arvidson, R.E., Rica, J.W., Tréguier, E., d'Uston, C., Grant, J.A., McSween, J.Y., Golombek, M.P., Haldemann, A.F.C., de Souza, J.A., 2008. Structure, stratigraphy, and origin of Husband Hill, Columbia Hills, Gusev Crater, Mars. J. Geophys. Res. E Planets 113, 1–14. doi:10.1029/2007JE003041

McHenry, L.J., Carson, G.L., Dixon, D.T., Vickery, C.L., 2017. Secondary minerals associated with Lassen fumaroles and hot springs: Implications for martian hydrothermal deposits. Am. Mineral. 102, 1418–1434. doi:10.2138/am-2017-5839

McSween, H., 2015. Petrology on Mars. Am. Mineral. 100, 2380–2395.

McSween, H.Y., Ruff, S.W., Morris, R. V., Gellert, R., Klingelhöfer, G., Christensen, P.R., McCoy, T.J., Ghosh, A., Moersch, J.M., Cohen, B.A., Rogers, A.D., Schröder, C., Squyres, S.W., Crisp, J., Yen, A., 2008. Mineralogy of volcanic rocks in Gusev Crater, Mars: Reconciling Mössbauer, Alpha Particle X-Ray Spectrometer, and Miniature Thermal Emission Spectrometer spectra. J. Geophys. Res. E Planets 113, 1–14. doi:10.1029/2007JE002970

McSween, H.Y., Wyatt, M.B., Gellert, R., Bell, I.F., Morris, R. V., Herkenhoff, K.E., Crumpler, L.S., Milam, K.A., Stockstill, K.R., Tornabene, L.L., Arvidson, R.E., Bartlett, P., Blaney, D., Cabrol, N.A., Christensen, P.R., Clark, B.C., Crisp, J.A., Des Marais, D.J., Economou, T., Farmer, J.D., Farrand, W., Ghosh, A., Golombek, M., Gorevan, S., Greeley, R., Hamilton, V.E., Johnson, J.R., Joliff, B.L., Klingelh??fer, G., Knudson, A.T., McLennan, S., Ming, D., Moersch, J.E., Rieder, R., Ruff, S.W., Schr??rder, C., de Souza, J.A., Squyres, S.W., W??nke, H., Wang, A., Yen, A., Zipfel, J., 2006. Characterization and petrologic interpretation of olivine-rich basalts at Gusev Crater, Mars. J. Geophys. Res. E Planets 111, 1–17. doi:10.1029/2005JE002477

Ming, D.W., Gellert, R., Morris, R. V., Arvidson, R.E., Brückner, J., Clark, B.C., Cohen, B.A., D'Uston, C., Economou, T., Fleischer, I., Klingelhöfer, G., McCoy, T.J., Mittlefehldt, D.W., Schmidt, M.E., Schröder, C., Squyres, S.W., Tréguier, E., Yen, A.S., Zipfel, J., 2008. Geochemical properties of rocks and soils in Gusev Crater, Mars: Results of the Alpha Particle X-Ray Spectrometer from Cumberland Ridge to Home Plate. J. Geophys. Res. E Planets 113. doi:10.1029/2008JE003195

Morris, R. V., Klingelhofer, G., Schroder, C., Fleischer, I., Ming, D.W., Yen, A.S., Gellert, R., Arvidson, R.E., Rodionov, D.S., Crumpler, L.S., Clark, B.C., Cohen, B.A., McCoy, T.J., Mittlefehldt, D.W., Schmidt, M.E., De Souza, J.A., Squyres, S.W., 2008. Iron mineralogy and aqueous alteration from Husband Hill through Home Plate at Gusev Crater, Mars: Results from the Mossbauer instrument on the Spirit Mars Exploration Rover. J. Geophys. Res. E Planets 113. doi:10.1029/2008JE003201

Mutonga, M.W., Sveinbjornsdottir, A., Gislason, G., Amannsson, H., 2010. The Isotopic and Chemical Characteristics of Geothermal Fluids in Hengill Area, SW-Iceland (Hellisheidi, Hveragerdi and Nesjavellir Fields). Proc. World Geotherm. Congr. 2010 25–29.

Nicolau, C., Reich, M., Lynne, B., 2014. Physico-chemical and environmental controls on siliceous sinter formation at the high-altitude El Tatio geothermal field, Chile. J. Volcanol. Geotherm. Res. 282, 60–76. doi:10.1016/j.jvolgeores.2014.06.012

Nixon, S.L., Cousins, C.R., Cockell, C.S., 2013. Plausible microbial metabolisms on Mars. Astron. Geophys. 54, 13–16. doi:10.1093/astrogeo/ats034

Rice, M.S., Bell, J.F., Cloutis, E.A., Wang, A., Ruff, S.W., Craig, M.A., Bailey, D.T., Johnson, J.R., de Souza, P.A., Farrand, W.H., 2010. Silica-rich deposits and hydrated minerals at Gusev Crater, Mars: Vis-NIR spectral characterization and regional mapping. Icarus 205, 375–395. doi:10.1016/j.icarus.2009.03.035

Rieder, R., Gellert, R., Anderson, R.C., Br??ckner, J., Clark, B.C., Dreibus, G., Economou, T., Klingelh??fer, G., Lugmair, G.W., Ming, D.W., Squyres, S.W., D'Uston, C., W??nke, H., Yen, A., Zipfel, J., 2004. Chemistry of rocks and soils at Meridiani Planum from the Alpha Particle X-ray Spectrometer. Science (80-.). 306, 1746–1749. doi:10.1126/science.1104358

Ruff, S.W., Farmer, J.D., 2016. Silica deposits on Mars with features resembling hot spring biosignatures at El Tatio in Chile. Nat. Commun. 7, 1–10. doi:10.1038/ncomms13554

Ruff, S.W., Farmer, J.D., Calvin, W.M., Herkenhoff, K.E., Johnson, J.R., Morris, R. V., Rice, M.S., Arvidson, R.E., Bell, J.F., Christensen, P.R., Squyres, S.W., 2011. Characteristics, distribution, origin, and significance of opaline silica observed by the Spirit rover in Gusev crater, Mars. J. Geophys. Res. E Planets 116. doi:10.1029/2010JE003767

Schmidt, M.E., Campbell, J.L., Gellert, R., Perrett, G.M., Treiman, A.H., Blaney, D.L., Olilla, A., Calef, F.J., Edgar, L., Elliott, B.E., Grotzinger, J., Hurowitz, J., King, P.L., Minitti, M.E., Sautter, V., Stack, K., Berger, J.A., Bridges, J.C., Ehlmann, B.L., Forni, O., Leshin, L.A., Lewis, K.W., McLennan, S.M., Ming, D.W., Newsom, H., Pradler, I., Squyres, S.W., Stolper, E.M., Thompson, L., Vanbommel, S., Wiens, R.C., 2014. Geochemical diversity in first rocks examined by the curiosity rover in gale crater: Evidence for and significance of an alkali and volatile-rich igneous source. J. Geophys. Res. E Planets 119, 64–81. doi:10.1002/2013JE004481

Schmidt, M.E., Farrand, W.H., Johnson, J.R., Schröder, C., Hurowitz, J.A., McCoy, T.J., Ruff, S.W., Arvidson, R.E., Des Marais, D.J., Lewis, K.W., Ming, D.W., Squyres, S.W., de Souza, P.A., 2009. Spectral, mineralogical, and geochemical variations across Home Plate, Gusev Crater, Mars indicate high and low temperature alteration. Earth Planet. Sci. Lett. 281, 258–266. doi:10.1016/j.epsl.2009.02.030

Schmidt, M.E., Ruff, S.W., McCoy, T.J., Farrand, W.H., Johnson, J.R., Gellert, R., Ming, D.W., Morris, R. V., Cabrol, N., Lewis, K.W., Schroeder, C., 2008. Hydrothermal origin of halogens at Home Plate, Gusev Crater. J. Geophys. Res. E Planets 113, 1–21. doi:10.1029/2007JE003027

Squyres, S.W., Aharonson, O., Clark, B.C., Cohen, B.A., Crumpler, L., de Souza, P.A., Farrand, W.H., Gellert, R., Grant, J., Grotzinger, J.P., Haldemann, A.F.C., Johnson, J.R., Klingelhofer, G., Lewis, K.W., Li, R., McCoy, T., McEwan, A.S., McSween, H.Y., Ming, D.W., Moore, J.M., Parker, T.J., Rice Jr, J.W., Ruff, S., Schmidt, M., Schroder, C., Soderblom, L.A., Yen, A., 2007. Pyroclastic Activity at Home Plate in Gusev Crater, Mars. Science (80-.). 316, 738–742.

Squyres, S.W., Arvidson, R.E., Ruff, S., Gellert, R., Morris, R. V., Ming, D.W., Crumpler, L., Farmer, J.D., Marais, D.J. Des, Yen, A., McLennan, S.M., Calvin, W., III, J.F.B., Clark, B.C., Wang, A., McCoy, T.J., Schmidt, M.E., Jr., P.A. de S., 2008. Detection of Silica-Rich deposits on Mars. Science (80-.). 320, 1063–1068.

Squyres, S.W., Grotzinger, J.P., Arvidson, R.E., Bell, J.F., Calvin, W., Christensen, P.R., Clark, B.C., Crisp, J.A., Farrand, W.H., Herkenhoff, K.E., Johnson, J.R., Klingelhöfer, G., Knoll, A.H., McLennan, S.M., McSween, H.Y., Morris, R. V., Rice, J.W., Rieder, R., Soderblom, L.A., 2004. In situ evidence for an ancient aqueous environment at Meridiani Planum,

Mars. Science (80-.). 306, 1709–1714. doi:10.1126/science.1104559

Stefánsson, A., Keller, N.S., Robin, J.G., Kaasalainen, H., Björnsdóttir, S., Pétursdóttir, S., Jóhannesson, H., Hreggvidsson, G.Ó., 2016. Quantifying mixing, boiling, degassing, oxidation and reactivity of thermal waters at Vonarskard, Iceland. J. Volcanol. Geotherm. Res. 309, 53–62. doi:10.1016/j.jvolgeores.2015.10.014

Trønnes, R.G., 1990. Basaltic melt evolution of the Hengill volcanic system, SW Iceland, and evidence for clinopyroxene assimilation in primitive tholeiitic magmas. J. Geophys. Res. Solid Earth 95, 15893–15910. doi:10.1029/JB095iB10p15893

Verney-Carron, A., Vigier, N., Millot, R., Hardarson, B.S., 2015. Lithium isotopes in hydrothermally altered basalts from Hengill (SW Iceland). Earth Planet. Sci. Lett. 411, 62–71. doi:10.1016/j.epsl.2014.11.047

Wang, A., Bell, I.F., Li, R., Johnson, J.R., Farrand, W.H., Cloutis, E.A., Arvidson, R.E., Crumpler, L., Squyres, S.W., McLennan, S.M., Herkenhoff, K.E., Ruff, S.W., Knudson, A.T., Chen, W., Greenberger, R., 2008. Light-toned salty soils and coexisting Si-rich species discovered by the Mars Exploration Rover Spirit in Columbia Hills. J. Geophys. Res. E Planets 113, 1–35. doi:10.1029/2008JE003126

Wangombe, P.W., 1987. MAPPING AT GRENSDALUR-REYKJADALUR AREA. UNU Geothermal Training Programme, National Energy Authority.

Westall, F., Loizeau, D., Foucher, F., Bost, N., Betrand, M., Vago, J., Kminek, G., 2013. Habitability on Mars from a Microbial Point of View. Astrobiology 13, 887–897. doi:10.1089/ast.2013.1000

Yen, A.S., Morris, R. V., Clark, B.C., Gellert, R., Knudson, A.T., Squyres, S., Mittlefehldt, D.W., Ming, D.W., Arvidson, R., McCoy, T., Schmidt, M., Hurowitz, J., Li, R., Johnson, J.R., 2008. Hydrothermal processes at Gusev Crater: An evaluation of Paso Robles class soils. J. Geophys. Res. E Planets 113, 1–19. doi:10.1029/2007JE002978

Appendix A

Field Photos

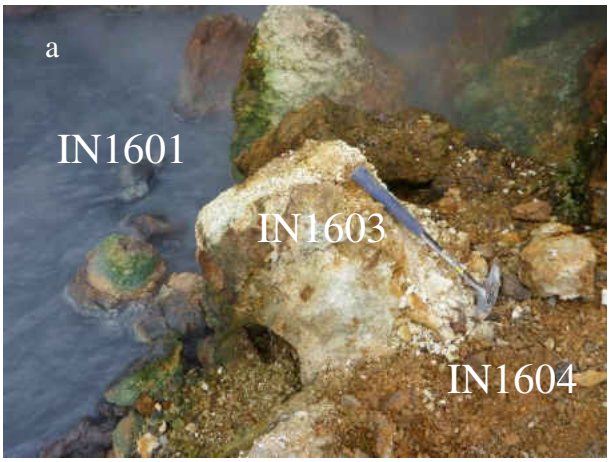

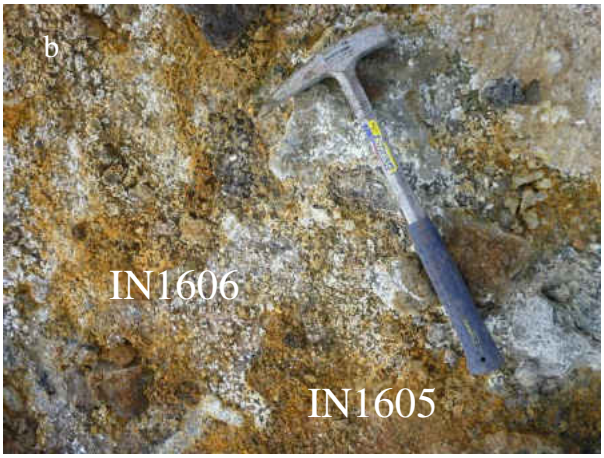

Figure 34- Northern near-neutral spring (IN1601, 82.2°C). a) White heavily leached rock (IN1603, 21.7°C) and soft orange coating (IN1604, 22.9°C). b) Orange crinkly precipitate (IN1605, 42.8°C) and white cauliflower-like precipitates (IN1606, 46.8°C). c) Dark grey soil at a few cm depth (IN1707, 90.3°C).

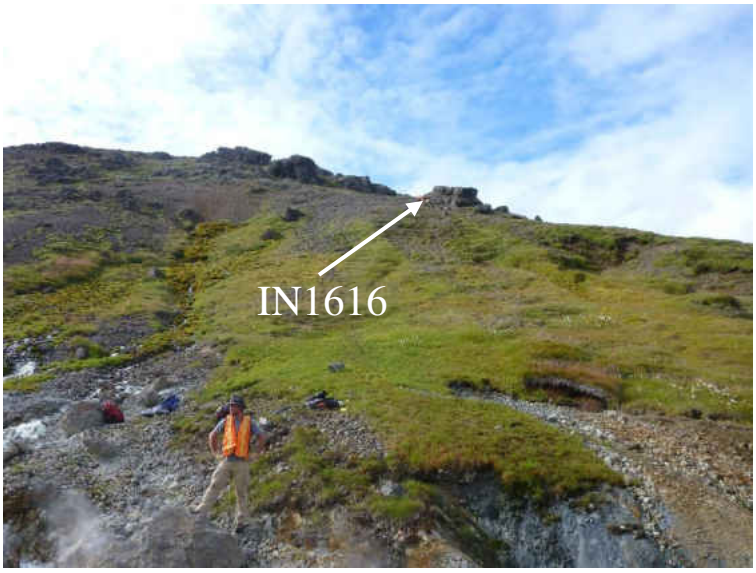

Figure 35- Ridgeline where substrate was collected (IN1616, ambient temperature).

Figure 36- Bubbling hot spring in between the red and white streams (IN1709, 81.7°C).

Figure 37- Older travertine deposits from the neutral travertine spring (IN1703, ambient temperature).

Appendix B

Supplementary SEM Images

Figure 38- Unusual, possibly biological structures in the siliceous edge of the travertine sample.

Figure 39- Biogenic tubules with smaller abiogenic siliceous tubes adhered to the sides. Located throughout the travertine.

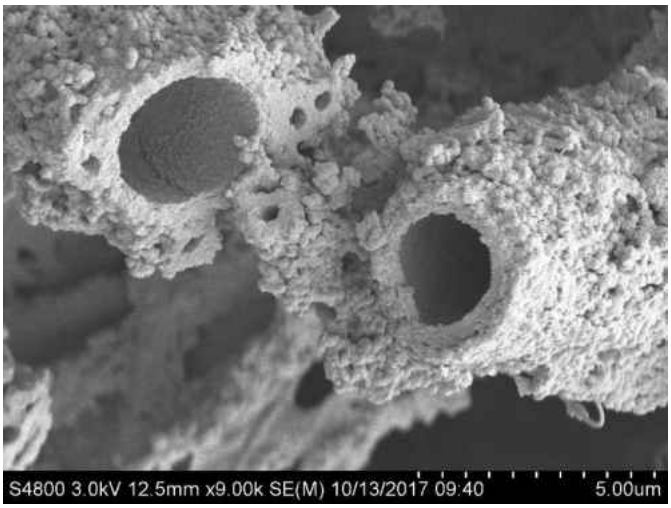

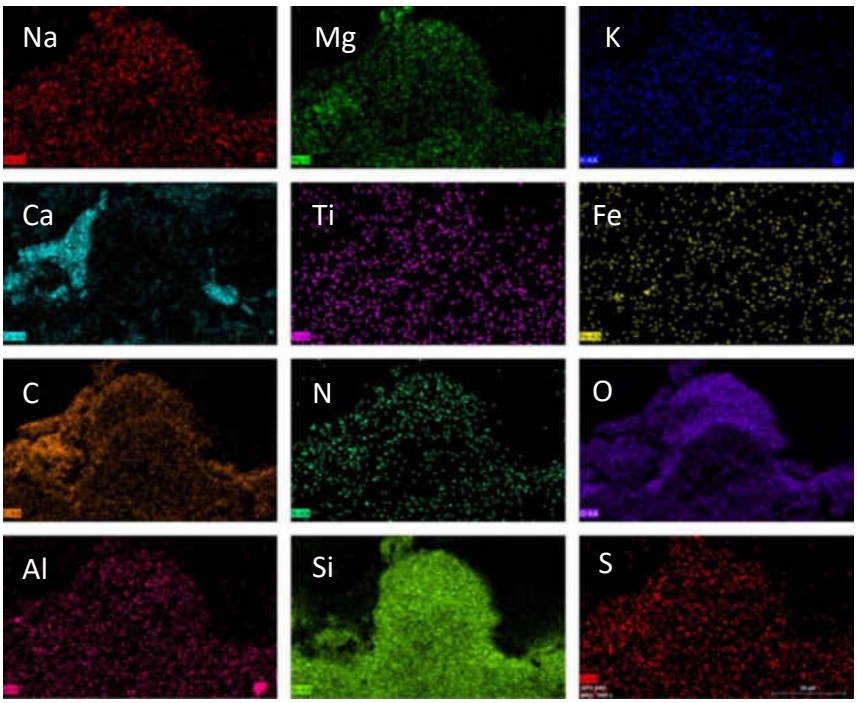

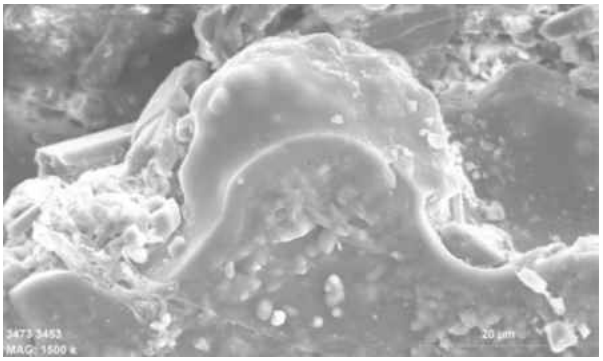

Figure 40- EDS element map of an amorphous, massive concretion. Ca is enriched on the side of the main feature, due to crystalline aragonite. The main feature contains high concentrations of both Si and O, indicating that the amorphous concretion is primarily silica.

Appendix C

Detailed List of Samples

	Site	Sample	GPS Coordinates North	West
2013	Hveragerdi sinter spring	IH1311		
		IH1312		
		IH1313		
		IH1314	64.09719	21.27459
2016	Northern near-neutral hot spring	IN1601	64.09718	21.27452
		IN1603	64.09718	21.27452
		IN1604	64.09718	21.27452
		IN1605	64.09718	21.27452
		IN1606	64.09718	21.27452
		IN1607	64.09718	21.27452
	Acidic and near-neutral springs and streams	IN1608	64.08691	21.27097
		IN1609	64.08691	21.27097
		IN1610	64.08688	21.27068
		IN1611	64.08688	21.27068
		IN1612	64.08688	21.27068
		IN1613	64.08688	21.27068
		IN1614	64.08688	21.27068
		IN1615		
2017	Southern neutral hot spring and acidic mud pot	IN1701	64.08246	21.26731
		IN1702	64.08246	21.26731
		IN1703	64.08246	21.26731
		IN1704	64.08246	21.26731
		IN1705	64.0818	21.26582
		IN1706	64.0818	21.26582
		IN1707	64.0818	21.26582
		IN1708	64.0818	21.26582
	Acidic and near-neutral springs and streams	IN1709	64.0868	21.27102
		IN1710	64.08688	21.08688
		IN1711	64.08688	21.08688
		IN1712	64.08691	21.27086
		IN1713	64.08691	21.27086
		IN1714	64.08684	21.27171
		IN1715	64.08704	21.27071
		IN1716	64.08688	21.2707
		IN1717	64.08626	21.27166
		IN1718	64.08626	21.27166
	Hveragerdi sinter	IH1701	64.02549	21.21257
		IH1702	64.02549	21.21257

Table 12- List of all samples and GPS coordinates. Samples separated by location and thermal feature. Light blue- northern hot spring, yellow- near neutral stream, red- acidic stream, green- confluence water, orange- neutral travertine-depositing hot spring, dark blue- acidic mud pot, gray- hot spring, dark red- acidic mud pot uphill from hydrothermal streams, bright green- neutral sinter depositing hot spring in the Hveragerdi geothermal field.

Table 13- Detailed list of all mud, soil, precipitate, and substrate samples separated by location, thermal feature, sample site, type of sample, temperature, and mineral assemblages present. Minerals are presented in alphabetical order. Amb- Ambient temperature.

Sample	Location	Thermal feature	Type	T (°C)	Mineral Assemblage
Northern near-neutral hot spring					
IN1603	Nesjavellir	Hot spring	Soil	21.7	Amorphous silica, Anatase. Tridymite
IN1604	Nesjavellir	Hot spring	Soil	22.9	Montmorillonite, Kaolinite
IN1605	Nesjavellir	Fumarole	Precipitate	42.8	Alunogen, Amorphous Silica, Anatase, Gypsum, Montmorillonite, Natrojarosite
IN1606	Nesjavellir	Fumarole	Precipitate	46.8	Halotrichite/Pickeringite
IN1607	Nesjavellir	Fumarole	Soil	90.3	Alunogen, Montmorillonite, Plagioclase, Pyrite
Acidic and near-neutral streams					
IN1609	Nesjavellir	Hydrothermal stream	Precipitate	15	Montmorillonite, Sulfur
IN1710	Nesjavellir	Hydrothermal stream	Precipitate	9.3	Montmorillonite, Sulfur
IN1713	Nesjavellir	Fumarole	Precipitate	57.1	Magnesiocopiapite, Pickeringite
IN1611	Nesjavellir	Hydrothermal stream	Precipitate	59.3	Possible nanophase Fe-oxides
IN1612	Nesjavellir	Fumarole	Soil	59.3	Anatase, Kaolinite, Pyrite
IN1614	Nesjavellir	Mud pot	Precipitate	68.5	Aluminite, Alunogen, Amorphous silica, Marcasite, Melanterite, Pyrite, Rhomboclase, Sulfur
IN1718	Nesjavellir	Mud pot	Mud	94.9	Alunogen, Barite, Kaolinite, Plagioclase, Pyrite, Sulfur
IN1616	Nesjavellir	-	Substrate	Amb	Plagioclase, Clinopyroxene
Travertine spring and associated mud pot					
IN1702	Nesjavellir	Hot spring	Precipitate	68	Amorphous silica, Aragonite, Calcite
IN1703	Nesjavellir	Hot spring	Precipitate	15	Aragonite, Calcite
IN1704	Nesjavellir	Hot spring	Precipitate	15	Aragonite, Calcite
IN1706	Nesjavellir	Mud pot	Mud pot	82.6	Gypsum, Pyrite, Sulfur
IN1707	Nesjavellir	Mud pot	Soil	92.1	Amorphous silica, anatase
IN1708	Nesjavellir	Mud pot	Soil	44	Kaolinite
Sinter hot spring					
IH1311	Hveragerdi	Hot spring	Precipitate	90	Amorphous silica
IH1313	Hveragerdi	Hot spring	Soil	90	Amorphous silica, Kaolinite
IH1314	Hveragerdi	Hot spring	Precipitate	10.3	Amorphous silica, Calcite, Halite
IH1702	Hveragerdi	Hot spring	Precipitate	71.4	Gypsum, Pyrite, Sulfur